

Article

A Generalized Strain Energy-Based Homogenization Method for 2-D and 3-D Cellular Materials with and without Periodicity Constraints [†]

Ahmad I. Gad and Xin-Lin Gao * 

Department of Mechanical Engineering, Southern Methodist University, Dallas, TX 75275-0337, USA; aigad@mail.smu.edu

* Correspondence: xlgao@smu.edu; Tel.: +1-214-768-1378

[†] This paper is submitted for the Special Issue on Metamaterials and Symmetry.

Abstract: A generalized strain energy-based homogenization method for 2-D and 3-D cellular materials with and without periodicity constraints is proposed using Hill's Lemma and the matrix method for spatial frames. In this new approach, the equilibrium equations are enforced at all boundary and interior nodes and each interior node is allowed to translate and rotate freely, which differ from existing methods where the equilibrium conditions are imposed only at the boundary nodes. The newly formulated homogenization method can be applied to cellular materials with or without symmetry. To illustrate the new method, four examples are studied: two for a 2-D cellular material and two for a 3-D pentamode metamaterial, with and without periodic constraints in each group. For the 2-D cellular material, an asymmetric microstructure with or without periodicity constraints is analyzed, and closed-form expressions of the effective stiffness components are obtained in both cases. For the 3-D pentamode metamaterial, a primitive diamond-shaped unit cell with or without periodicity constraints is considered. In each of these 3-D cases, two different representative cells in two orientations are examined. The homogenization analysis reveals that the pentamode metamaterial exhibits the cubic symmetry based on one representative cell, with the effective Poisson's ratio $\bar{\nu}$ being nearly 0.5. Moreover, it is revealed that the pentamode metamaterial with the cubic symmetry can be tailored to be a rubber-like material (with $\bar{\nu} \cong 0.5$) or an auxetic material (with $\bar{\nu} < 0$).

Keywords: cellular material; strain energy-based homogenization; Hill's lemma; pentamode metamaterial; matrix method for spatial frames; effective elastic properties; stiffness matrix; periodic boundary conditions; auxetic material



Citation: Gad, A.I.; Gao, X.-L. A Generalized Strain Energy-Based Homogenization Method for 2-D and 3-D Cellular Materials with and without Periodicity Constraints. *Symmetry* **2021**, *13*, 1870. <https://doi.org/10.3390/sym13101870>

Academic Editor: Teik-Cheng Lim

Received: 18 July 2021

Accepted: 16 September 2021

Published: 4 October 2021

Publisher's Note: MDPI stays neutral with regard to jurisdictional claims in published maps and institutional affiliations.



Copyright: © 2021 by the authors. Licensee MDPI, Basel, Switzerland. This article is an open access article distributed under the terms and conditions of the Creative Commons Attribution (CC BY) license (<https://creativecommons.org/licenses/by/4.0/>).

1. Introduction

Homogenization of materials with discrete microstructures is becoming increasingly important due to widespread applications of cellular structures and lattice-based metamaterials (e.g., [1–11]).

Various homogenization methods have been developed using classical elasticity. For example, Warren and Kraynik [12] proposed an analytical method to homogenize low-density open-cell foams based on solving force and moment equilibrium equations at joints. Tollenaere and Caillerie [13] used an asymptotic expansion method in homogenizing 2-D lattice truss structures. Li et al. [14] developed a micromechanics model and obtained closed-form formulas for predicting effective elastic properties of 3-D open-cell foams based on Castigliano's second theorem. Demiray et al. [15] homogenized 2-D and 3-D hyperelastic foams undergoing large deformations by employing a strain energy-based scheme and periodic conditions. Martinsson and Babuška [16] provided a homogenization method for materials with periodic truss and frame microstructures utilizing an asymptotic analysis built upon Fourier transforms. Freund et al. [17] presented a two-scale computational homogenization technique for 2-D cellular structures based on the virtual work principle.

Norris [18] proposed a homogenization method for periodic lattice structures and derived analytical formulas for effective properties of elastic networks, including pentamode metamaterials. Ongaro et al. [19] employed a strain energy-based approach to homogenize 2-D cellular structures of honeycomb cells filled with an elastic material. Ai and Gao [20] provided an analytical model for predicting effective elastic properties of 2-D periodic star-shaped re-entrant lattice structures with the orthotropic symmetry and negative Poisson's ratios by using Castigliano's second theorem and the Timoshenko beam theory. Materials with negative Poisson ratios are also known as auxetic materials, which have emerged as a class of metamaterials that can find important engineering applications (e.g., [6,20–26]). Recently, Czarnecki and Łukasiak [27] applied the asymptotic homogenization method for periodic media to estimate effective moduli of 2-D auxetic cellular materials, which were also compared with those obtained through optimization.

Higher-order elasticity theories have also been applied to develop models for homogenizing 2-D and 3-D cellular materials (e.g., [11,28–34]).

In the current study, a generalized strain energy-based homogenization method for 2-D and 3-D cellular materials with and without periodicity constraints is developed, which is built on classical elasticity and has no restriction on shape, symmetry or number of struts in a unit cell. In this new approach, the nodal equilibrium equations are enforced at all boundary and interior nodes, unlike in existing classical elasticity-based methods where the nodal equilibrium is imposed only at the boundary nodes and, as a result, the equilibrium equations are often not satisfied at the interior nodes by the approximate solutions obtained (e.g., [35]).

The rest of the paper is organized as follows. In Section 2, the generalized strain energy-based homogenization method is formulated for cellular materials with and without periodicity constraints. In Section 3, the newly proposed method is applied to homogenize 2-D and 3-D cellular materials in four example problems, which leads to closed-form formulas for effective elastic stiffness and compliance components. In Section 4, the paper concludes with a summary.

2. Generalized Strain Energy-Based Homogenization Method

2.1. Matrix Method for Spatial Frames

According to the matrix method for spatial frames (e.g., [36,37]), each frame member is regarded as weightless and loaded only at its two end points (nodes). It is rigidly connected to other members at the two end nodes, each having six degrees of freedom—three translational and three rotational displacements—if unconstrained.

For a 3-D frame member with two end nodes I and J , denoted as " I, J " and shown in Figure 1, which is made from an isotropic linear elastic material and has a uniform circular cross-section, the stiffness matrix is given by

$$\mathbf{k} = \begin{bmatrix} \mathbf{k}_{II} & \mathbf{k}_{IJ} \\ \mathbf{k}_{JI} & \mathbf{k}_{JJ} \end{bmatrix}, \quad (1)$$

where the 6×6 sub-stiffness matrix \mathbf{k}_{IJ} represents the force at node I due to a unit displacement at node J .

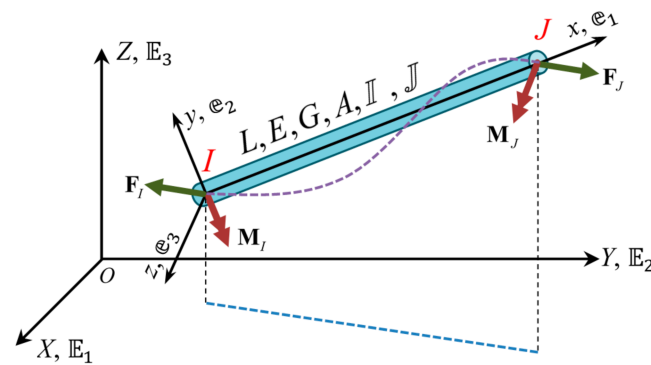


Figure 1. 3-D frame member.

In the local coordinate system $\{x, y, z\}$ with the base vectors $\{e_1, e_2, e_3\}$, as shown in Figure 1, the sub-stiffness matrices can be written as (e.g., [37])

$$\mathbf{k}_{II} = \begin{bmatrix} k_a & 0 & 0 & 0 & 0 & 0 \\ 0 & k_s & 0 & 0 & 0 & \frac{L}{2}k_s \\ 0 & 0 & k_s & 0 & -\frac{L}{2}k_s & 0 \\ 0 & 0 & 0 & k_t & 0 & 0 \\ 0 & 0 & -\frac{L}{2}k_s & 0 & k_b & 0 \\ 0 & \frac{L}{2}k_s & 0 & 0 & 0 & k_b \end{bmatrix}, \quad \mathbf{k}_{JJ} = \begin{bmatrix} k_a & 0 & 0 & 0 & 0 & 0 \\ 0 & k_s & 0 & 0 & 0 & -\frac{L}{2}k_s \\ 0 & 0 & k_s & 0 & \frac{L}{2}k_s & 0 \\ 0 & 0 & 0 & k_t & 0 & 0 \\ 0 & 0 & \frac{L}{2}k_s & 0 & k_b & 0 \\ 0 & -\frac{L}{2}k_s & 0 & 0 & 0 & k_b \end{bmatrix},$$

$$\mathbf{k}_{IJ} = \mathbf{k}_{JI}^T = \begin{bmatrix} -k_a & 0 & 0 & 0 & 0 & 0 \\ 0 & -k_s & 0 & 0 & 0 & \frac{L}{2}k_s \\ 0 & 0 & -k_s & 0 & -\frac{L}{2}k_s & 0 \\ 0 & 0 & 0 & -k_t & 0 & 0 \\ 0 & 0 & \frac{L}{2}k_s & 0 & \frac{L^2}{2}k_s - k_b & 0 \\ 0 & -\frac{L}{2}k_s & 0 & 0 & 0 & \frac{L^2}{2}k_s - k_b \end{bmatrix}, \quad (2)$$

where the superscript “*T*” denotes the transpose of the matrix, *L* is the length of the frame member, and *k_a*, *k_s*, *k_b* and *k_t* are, respectively, the axial stiffness along the *x*-axis, transverse shear stiffness about the *y*- or *z*-axis, bending stiffness about the *y*- or *z*-axis, and torsional stiffness about the *x*-axis. When the Timoshenko beam theory is used [37],

$$k_a = \frac{EA}{L}, \quad k_s = \frac{12\eta EGA\mathbb{I}}{12E\mathbb{I}L + \eta AGL^3}, \quad k_b = \frac{4E\mathbb{I}(3E\mathbb{I} + \eta GAL^2)}{12E\mathbb{I}L + \eta AGL^3}, \quad k_t = \frac{G\mathbb{J}}{L}, \quad (3)$$

which can be reduced to those based on the Bernoulli-Euler beam theory given by

$$k_a = \frac{EA}{L}, \quad k_s = \frac{12E\mathbb{I}}{L^3}, \quad k_b = \frac{4E\mathbb{I}}{L}, \quad k_t = \frac{G\mathbb{J}}{L}, \quad (4)$$

where *E* and *G* are, respectively, Young’s modulus and the shear modulus of the member material, η is the shear correction factor, and *A*, \mathbb{I} and \mathbb{J} are, respectively, the area, second moment of area and polar second moment of area of the circular cross-section member with the diameter *d* known as

$$A = \frac{\pi d^2}{4}, \quad \mathbb{I} = \frac{\pi d^4}{64}, \quad \mathbb{J} = \frac{\pi d^4}{32}. \quad (5)$$

Based on the arrangement of the sub-stiffness matrices in Equation (1), the nodal displacement vector of the member “*I, J*” in the local coordinate system can be written as

$$\Delta = \{ \mathbf{u}_I \quad \theta_I \quad \mathbf{u}_J \quad \theta_J \}^T, \quad (6)$$

where \mathbf{u}_I and \mathbf{u}_J represent, respectively, the displacement vectors at nodes I and J , and θ_I and θ_J denote, respectively, the rotation vectors at nodes I and J .

In the global coordinate system $\{X, Y, Z\}$ with the unit vectors $\{\mathbb{E}_1, \mathbb{E}_2, \mathbb{E}_3\}$ shown in Figure 1, which is independent of the frame (strut) orientation, the nodal displacement vector of the member “ I, J ” becomes

$$\mathbf{D} = \{ u_{XI} \ u_{YI} \ u_{ZI} \ \theta_{XI} \ \theta_{YI} \ \theta_{ZI} \ u_{XJ} \ u_{YJ} \ u_{ZJ} \ \theta_{XJ} \ \theta_{YJ} \ \theta_{ZJ} \}^T, \quad (7)$$

which is related to Δ (see Equation (6)) through

$$\mathbf{D} = \mathbf{Q}^T \Delta, \quad (8)$$

where

$$\mathbf{Q} = \begin{bmatrix} \mathbf{Q} & \mathbf{0} & \mathbf{0} & \mathbf{0} \\ \mathbf{0} & \mathbf{Q} & \mathbf{0} & \mathbf{0} \\ \mathbf{0} & \mathbf{0} & \mathbf{Q} & \mathbf{0} \\ \mathbf{0} & \mathbf{0} & \mathbf{0} & \mathbf{Q} \end{bmatrix}, \quad \mathbf{Q} = \cos(\mathbf{e}_i, \mathbb{E}_j) \mathbb{E}_i \otimes \mathbb{E}_j, \quad (9)$$

in which \mathbf{Q} is the orthogonal coordinate transformation matrix from the local coordinate system $\{x, y, z\}$ to the global coordinate system $\{X, Y, Z\}$ (i.e., $\mathbb{E}_i = \mathbf{Q} \mathbf{e}_i$), and the summation on i and j (with $i, j \in \{1, 2, 3\}$) is implied. Note that \mathbf{Q} is also proper orthogonal with $\mathbf{Q}^{-1} = \mathbf{Q}^T$ and $\det \mathbf{Q} = 1$, where the superscript “ $-$ ” denotes the inverse of the matrix.

The nodal force vector of the member “ I, J ” that satisfies the equilibrium is given by (e.g., [37])

$$\mathbf{\Gamma} = \mathbf{k} \Delta = \{ \mathbf{F}_I \ \mathbf{M}_I \ \mathbf{F}_J \ \mathbf{M}_J \}^T, \quad (10)$$

or in terms of the components in the local coordinate system,

$$\mathbf{\Gamma} = \{ F_{xI} \ F_{yI} \ F_{zI} \ M_{xI} \ M_{yI} \ M_{zI} \ F_{xJ} \ F_{yJ} \ F_{zJ} \ M_{xJ} \ M_{yJ} \ M_{zJ} \}^T, \quad (11)$$

where $\mathbf{F}_I = F_{iI} \mathbf{e}_i$, $\mathbf{M}_I = M_{iI} \mathbf{e}_i$ and $\mathbf{F}_J = F_{iJ} \mathbf{e}_i$, $\mathbf{M}_J = M_{iJ} \mathbf{e}_i$ are, respectively, the force and moment vectors at nodes I and J . Note that the summation on $i \in \{1, 2, 3\}$ is implied here.

In the global coordinate system, the nodal force vector for the member “ I, J ” can be obtained from Equations (8) and (10) as

$$\mathbf{S} = \mathbf{Q}^T \mathbf{\Gamma} = \mathbf{Q}^T \mathbf{k} \Delta = \mathbf{Q}^T \mathbf{k} \mathbf{Q} \mathbf{D} = \mathbf{K} \mathbf{D}, \quad (12)$$

where

$$\mathbf{K} = \mathbf{Q}^T \mathbf{k} \mathbf{Q} \quad (13)$$

is the stiffness matrix of the member “ I, J ” in the global coordinate system $\{X, Y, Z\}$.

For a cellular material containing W frame members, the total strain energy is given by

$$\mathbb{U} = \frac{1}{2} \sum_{n=1}^W \mathbf{D}_n^T \mathbf{K}_n \mathbf{D}_n, \quad (14)$$

where $n \in \{1, 2, \dots, W\}$ represents the n th frame member, and

$$\mathbf{K}_n = \mathbf{Q}_n^T \mathbf{k}_n \mathbf{Q}_n. \quad (15)$$

2.2. Hill's Lemma

Hill's lemma [38] enables the prediction of effective properties of a heterogeneous material through constructing a homogeneous comparison solid based on the strain energy equivalence (e.g., [39–41]).

For the Cauchy continuum, Hill's lemma reads (e.g., [38,39,42,43])

$$\langle \boldsymbol{\sigma} : \boldsymbol{\varepsilon} \rangle - \boldsymbol{\Sigma} : \mathbf{E} = \frac{1}{V} \int_{\partial \Omega} (\mathbf{u} - \mathbf{E} \mathbf{x}) \cdot [(\boldsymbol{\sigma} - \boldsymbol{\Sigma}) \mathbf{n}] dS, \quad (16)$$

where Ω is the region occupied by a heterogeneous material, $\partial\Omega$ is the closed surface of Ω , V is the volume of Ω , dS is an area element on $\partial\Omega$, σ and ε are, respectively, the Cauchy stress and infinitesimal strain tensors, $\langle \cdot \rangle$ denotes the volume-averaged quantity, \mathbf{u} is the displacement vector, \mathbf{E} and Σ are, respectively, the volume-averaged (effective) stress and strain tensors, \mathbf{x} is the position vector, and \mathbf{n} is the unit outward normal to $\partial\Omega$. Note that $\langle \sigma : \varepsilon \rangle$ is twice of the volume-averaged strain energy density of the heterogeneous material, and $\Sigma : \mathbf{E}$ is twice of the volume-averaged strain energy density of the homogeneous comparison solid.

The Hill-Mandel condition requires that $\langle \sigma : \varepsilon \rangle - \Sigma : \mathbf{E} = 0$ for the strain energy equivalence, which leads to the following allowable boundary conditions:

$$\mathbf{u} = \mathbf{E}\mathbf{x} \quad \text{or} \quad \mathbf{t} = \sigma\mathbf{n} = \Sigma\mathbf{n} \quad \text{on } \partial\Omega, \quad (17)$$

where \mathbf{t} is the Cauchy traction vector, and \mathbf{E} and Σ are, respectively, the prescribed (constant) strain and stress tensors given by

$$\mathbf{E} = \begin{bmatrix} \bar{\varepsilon}_{XX} & \bar{\varepsilon}_{XY} & \bar{\varepsilon}_{XZ} \\ \bar{\varepsilon}_{XY} & \bar{\varepsilon}_{YY} & \bar{\varepsilon}_{YZ} \\ \bar{\varepsilon}_{XZ} & \bar{\varepsilon}_{YZ} & \bar{\varepsilon}_{ZZ} \end{bmatrix}, \quad \Sigma = \begin{bmatrix} \bar{\sigma}_{XX} & \bar{\sigma}_{XY} & \bar{\sigma}_{XZ} \\ \bar{\sigma}_{XY} & \bar{\sigma}_{YY} & \bar{\sigma}_{YZ} \\ \bar{\sigma}_{XZ} & \bar{\sigma}_{YZ} & \bar{\sigma}_{ZZ} \end{bmatrix}, \quad (18)$$

in which the overhead bar represents the prescribed quantity.

From Equations (17) and (18), the displacement \mathbf{u} at each boundary node can be obtained. However, the rotation θ can vary independently at the boundary nodes while satisfying the moment equilibrium equations there (e.g., [44]). Accordingly, the displacement vector for the n th frame member " I, J " (with $n \in \{1, 2, \dots, W\}$) with the end nodes I and J both lying on the boundary of the cellular material can be rewritten as

$$\mathbf{D}_n = \{ \mathbf{E}\mathbf{X}_I \quad \theta_I \quad \mathbf{E}\mathbf{X}_J \quad \theta_J \}_n^T. \quad (19)$$

If node I lies on the boundary and node J is located in the interior, then the displacement vector for the n th frame member " I, J " has the form:

$$\mathbf{D}_n = \{ \mathbf{E}\mathbf{X}_I \quad \theta_I \quad \mathbf{u}_J \quad \theta_J \}_n^T. \quad (20)$$

Finally, if both the end nodes I and J lie in the interior of the cellular material, then

$$\mathbf{D}_n = \{ \mathbf{u}_I \quad \theta_I \quad \mathbf{u}_J \quad \theta_J \}_n^T. \quad (21)$$

2.3. Generalized Homogenization Method

Consider a general (asymmetric) 3-D cellular material with no periodicity, as shown in Figure 2. The cellular material is composed of P boundary frame members (struts), each of which has at least one node on the boundary, and Q interior struts, each of which has its two end nodes located inside the boundary. The cellular material also features N nodes that lie on the boundary and M nodes that are located inside the boundary. The cellular material can be completely characterized by N, M, P, Q and the coordinates of each node.

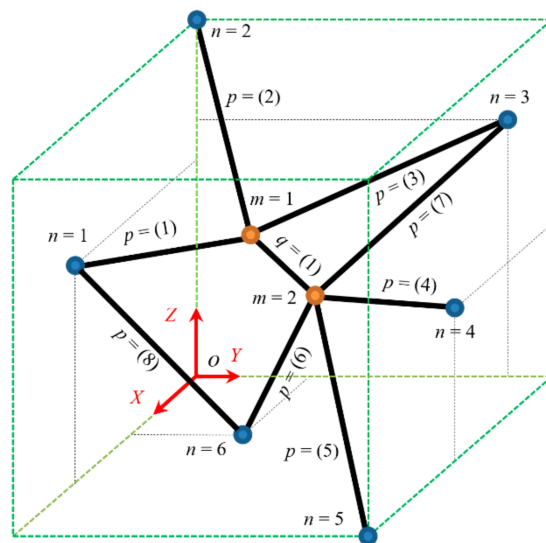


Figure 2. General 3-D cellular material.

To homogenize this cellular material with the equilibrium satisfied at all nodes (on the boundary and in the interior), the displacement boundary conditions in Equation (17) are prescribed for the boundary nodes. The remaining nodes inside the boundary are allowed to translate and rotate without any constraint. Thus, for the N boundary nodes, the following holds:

$$\mathbf{u}_n = \mathbf{E}\mathbf{X}_n \quad \text{and} \quad \mathbf{M}_n = \sum_{\bar{n}=1}^{\bar{N}} \mathbf{M}_{\bar{n}} = 0 \quad \text{on } \partial\Omega, \tag{22}$$

where $n (\in \{1, 2, \dots, N\})$ denotes the n th boundary node, and \bar{N} is the total number of struts emanating from the n th boundary node. This leaves the rotation vector at each boundary node, $\theta_n (n \in \{1, 2, \dots, N\})$, unspecified, while satisfying the nodal moment equilibrium. Then, the displacement vector for the p th boundary strut “ I, J ”, with node I lying on the boundary and node J located in the interior, can be obtained from Equations (20) and (22) as

$$\mathbf{D}_p = \left\{ \mathbf{E}\mathbf{X}_I \quad \theta_I \quad \mathbf{u}_J \quad \theta_J \right\}_p^T, \tag{23}$$

where $p (\in \{1, 2, \dots, P\})$ denotes the p th boundary strut.

From Equations (12) and (23), the force vector for the p th boundary strut “ I, J ” is given by

$$\mathbf{S}_p = \left\{ \begin{matrix} \mathbf{F}_I \\ \mathbf{M}_I \\ \mathbf{F}_J \\ \mathbf{M}_J \end{matrix} \right\}_p = \mathbf{K}_p \left\{ \begin{matrix} \mathbf{E}\mathbf{X}_I \\ \theta_I \\ \mathbf{u}_J \\ \theta_J \end{matrix} \right\}_p, \tag{24}$$

and from Equations (14) and (23), the total strain energy stored in the P boundary struts can be obtained as

$$\mathbb{U}_P = \frac{1}{2} \sum_{p=1}^P \left\{ \mathbf{E}\mathbf{X}_I \quad \theta_I \quad \mathbf{u}_J \quad \theta_J \right\}_p^T \mathbf{K}_p \left\{ \begin{matrix} \mathbf{E}\mathbf{X}_I \\ \theta_I \\ \mathbf{u}_J \\ \theta_J \end{matrix} \right\}_p. \tag{25}$$

On the other hand, the displacement vector for the q th interior strut “ I, J ”, with both nodes I and J located inside the boundary, can be obtained from Equation (21) as

$$\mathbf{D}_q = \{ \mathbf{u}_I \quad \boldsymbol{\theta}_I \quad \mathbf{u}_J \quad \boldsymbol{\theta}_J \}_q^T, \quad (26)$$

where $q (\in \{1, 2, \dots, Q\})$ denotes the q th interior strut.

From Equations (12) and (26), the force vector for the q th interior strut is given by

$$\mathbf{S}_q = \begin{Bmatrix} \mathbf{F}_I \\ \mathbf{M}_I \\ \mathbf{F}_J \\ \mathbf{M}_J \end{Bmatrix}_q = \mathbf{K}_q \begin{Bmatrix} \mathbf{u}_I \\ \boldsymbol{\theta}_I \\ \mathbf{u}_J \\ \boldsymbol{\theta}_J \end{Bmatrix}_q, \quad (27)$$

and from Equations (14) and (26), the total strain energy stored in the Q interior struts has the form:

$$\mathbb{U}_Q = \frac{1}{2} \sum_{q=1}^Q \{ \mathbf{u}_I \quad \boldsymbol{\theta}_I \quad \mathbf{u}_J \quad \boldsymbol{\theta}_J \}_q^T \mathbf{K}_q \begin{Bmatrix} \mathbf{u}_I \\ \boldsymbol{\theta}_I \\ \mathbf{u}_J \\ \boldsymbol{\theta}_J \end{Bmatrix}_q. \quad (28)$$

Then, the volume-averaged strain energy, called the strain energy density function, in the cellular material with P boundary struts and Q interior struts can be obtained as

$$u = \frac{\mathbb{U}}{V} = \frac{\mathbb{U}_P + \mathbb{U}_Q}{V}, \quad (29)$$

where V is the volume of the region enclosed by the bounding surface of the cellular material.

The strain energy density function u in Equation (29) contains a number of unknown displacement and rotation components. For a general 3-D case, these unknowns include $3N$ rotation components at the N boundary nodes ($\boldsymbol{\theta}_n; n \in \{1, 2, \dots, N\}$), $3M$ displacement components at the M interior nodes ($\mathbf{u}_m; m \in \{1, 2, \dots, M\}$), and $3M$ rotation components at the M interior nodes ($\boldsymbol{\theta}_m; m \in \{1, 2, \dots, M\}$). As a result, there are totally $6M + 3N$ unknown displacement and rotation components in u . Hence, an equal number of equations are required to solve for these unknowns so that the strain energy density function will not contain any undetermined displacement or rotation component.

Since each boundary node is allowed to rotate freely, enforcing the moment equilibrium at all the N boundary nodes provides $3N$ equations. These moment balance equations at the boundary nodes read

$$\mathbf{M}_n = \sum_{\bar{n}=1}^{\bar{N}} \mathbf{M}_{\bar{n}} = 0, \quad n \in \{1, 2, \dots, N\}. \quad (30)$$

Furthermore, since each interior node is allowed to translate and rotate without constraints, enforcing the force and moment equilibrium at all the M interior nodes gives $6M$ equations, which are

$$\mathbf{S}_m = \sum_{\bar{m}=1}^{\bar{M}} \mathbf{S}_{\bar{m}} = 0 \Leftrightarrow \mathbf{F}_m = \sum_{\bar{m}=1}^{\bar{M}} \mathbf{F}_{\bar{m}} = 0, \quad \mathbf{M}_m = \sum_{\bar{m}=1}^{\bar{M}} \mathbf{M}_{\bar{m}} = 0, \quad m \in \{1, 2, \dots, M\}, \quad (31)$$

where \bar{M} is the total number of struts emanating from the m th interior node.

Solving Equation (30) will yield $\boldsymbol{\theta}_n (n \in \{1, 2, \dots, N\})$ at the N boundary nodes, and solving Equation (31) will lead to \mathbf{u}_m and $\boldsymbol{\theta}_m (m \in \{1, 2, \dots, M\})$ at the M interior nodes. Substituting these determined kinematic variables into Equation (29) will give the strain

energy density function u in its final form without containing any unknown. The effective stiffness tensor can then be obtained from u as

$$\Sigma = \frac{\partial u}{\partial \mathbf{E}}, \quad \bar{\mathbf{C}} = \frac{\partial^2 u}{\partial \mathbf{E}^2}, \tag{32}$$

where \mathbf{E} and Σ are the constant strain and stress tensors defined in Equation (18), and $\bar{\mathbf{C}}$ is the effective stiffness (elasticity) tensor.

2.4. Extension to Periodic Materials

For periodic cellular materials, the homogenization can be performed using an extended version of the approach based on Hill’s lemma discussed in Section 2.3.

For a periodic material, Hill’s lemma given in Equation (16) can be extended to (e.g., [40])

$$\langle \sigma : \varepsilon \rangle - \Sigma : \mathbf{E} = \frac{1}{V} \int_{\partial\Omega} (\mathbf{u} - \mathbf{E}\mathbf{x} - \mathbf{u}^*) \cdot [(\sigma - \Sigma)\mathbf{n}] dS, \tag{33}$$

where \mathbf{u}^* is the periodic part of the displacement field, which is the same for each periodic pair of nodes on the unit cell boundary. Note that for each periodic pair of two boundary nodes the traction vector $\mathbf{t} = \sigma\mathbf{n}$ is anti-periodic with $\mathbf{t}^+ + \mathbf{t}^- = 0$ (e.g., [40,45,46]). Accordingly, the surface integral of the product $\mathbf{u}^* \cdot (\sigma - \Sigma)\mathbf{n}$ vanishes (e.g., [40,43]), and hence Equation (33) is equivalent to Equation (16). Applying the Hill-Mandel condition to Equation (33) then gives

$$\mathbf{u} = \mathbf{E}\mathbf{x} + \mathbf{u}^* \quad \text{or} \quad \sigma\mathbf{n} = \Sigma\mathbf{n} \quad \text{on } \partial\Omega \tag{34}$$

as the periodic BCs.

Consider a general 3-D periodic cellular material, with a unit cell shown in Figure 3a or Figure 3b. Each unit cell contains P boundary struts, each of which has one node on the boundary, and Q interior struts, each of which has its two nodes located inside the boundary. Each unit cell also includes B periodic pairs of nodes that lie on the boundary and M nodes that are located inside the boundary.

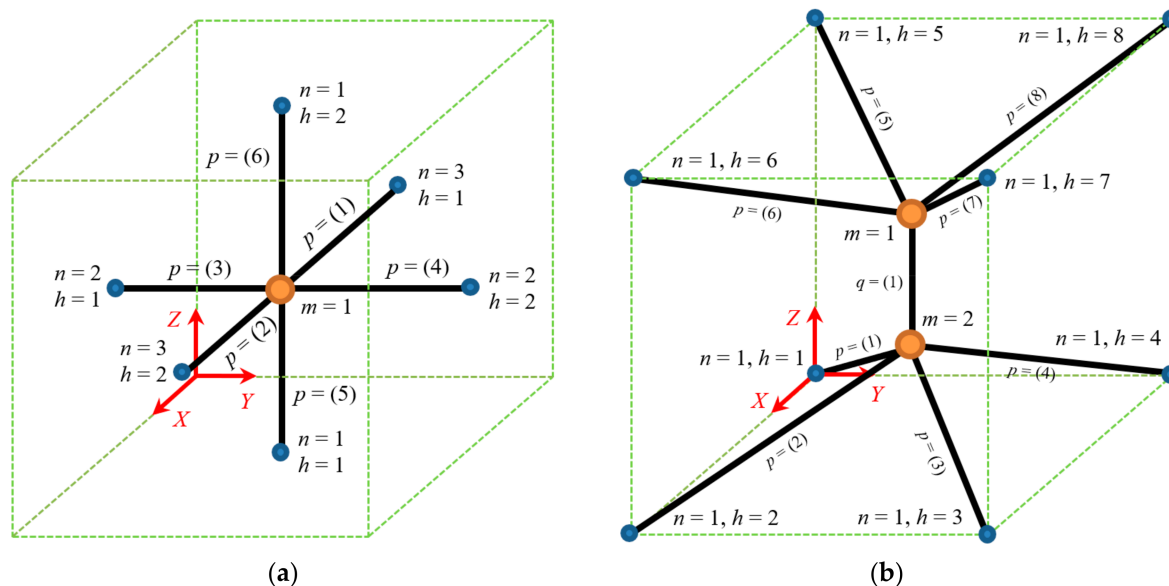


Figure 3. Periodic 3-D cellular material: (a) unit cell with three periodic pairs; (b) unit cell with one periodic pair.

A periodic pair can contain two or more boundary nodes, which depends on the unit cell structure. For example, the unit cell shown in Figure 3a possesses three periodic pairs ($B = 3$), each having two distinct nodes, while the unit cell in Figure 3b contains one

periodic pair ($B = 1$), with all the boundary nodes included in this pair. In general, for a periodic cellular material, a periodic pair can be defined as a collection of boundary nodes that satisfy the following conditions (e.g., [40,45]):

$$\mathbf{u}_1^* = \mathbf{u}_2^* = \cdots = \mathbf{u}_H^*, \quad \theta_1^* = \theta_2^* = \cdots = \theta_H^*, \quad (35)$$

$$\sum_{h=1}^H \mathbf{F}_h = 0, \quad \sum_{h=1}^H \mathbf{M}_h = 0, \quad (36)$$

where H represents the total number of nodes contained in the periodic pair.

The kinematic boundary conditions shown in Equation (34) can be extended to represent the periodic boundary conditions for a cellular material in the following form:

$$\mathbf{u}_n^h = \mathbf{E}\mathbf{X}_n^h + \mathbf{u}_n^*(\mathbf{X}) \quad \text{and} \quad \theta_n^h = \theta_n^*(\mathbf{X}) \quad \text{on} \quad \partial\Omega, \quad (37)$$

where $n (\in \{1, 2, \dots, B\})$ denotes the n th periodic pair of boundary nodes, $h (\in \{1, 2, \dots, H\})$ stands for the h th node in the n th periodic pair, and \mathbf{u}_n^* and θ_n^* ($n \in \{1, 2, \dots, B\}$) are, respectively, the periodic parts of the displacement and rotation, which are yet unknown. Using Equation (37) in Equation (20) gives the displacement vector for the p th boundary strut " I, J " (with $p \in \{1, 2, \dots, P\}$), with node I lying on the boundary and node J located inside, as

$$\mathbf{D}_p = \left\{ \mathbf{E}\mathbf{X}_I + \mathbf{u}_I^* \quad \theta_I^* \quad \mathbf{u}_J \quad \theta_J \right\}_p^T. \quad (38)$$

Then, it follows from Equations (12) and (38) that the force vector for the p th strut " I, J " has the form:

$$\mathbf{S}_p = \left\{ \begin{array}{c} \mathbf{F}_I \\ \mathbf{M}_I \\ \mathbf{F}_J \\ \mathbf{M}_J \end{array} \right\}_p = \mathbf{K}_p \left\{ \begin{array}{c} \mathbf{E}\mathbf{X}_I + \mathbf{u}_I^* \\ \theta_I^* \\ \mathbf{u}_J \\ \theta_J \end{array} \right\}_p, \quad (39)$$

and from Equations (14) and (38) that the total strain energy stored in the P boundary struts can be obtained as

$$\mathbb{U}_P = \frac{1}{2} \sum_{p=1}^P \left\{ \mathbf{E}\mathbf{X}_I + \mathbf{u}_I^* \quad \theta_I^* \quad \mathbf{u}_J \quad \theta_J \right\}_p^T \mathbf{K}_p \left\{ \begin{array}{c} \mathbf{E}\mathbf{X}_I + \mathbf{u}_I^* \\ \theta_I^* \\ \mathbf{u}_J \\ \theta_J \end{array} \right\}_p. \quad (40)$$

The displacement vector and force vector for the q th interior strut can be computed from Equations (26) and (27), respectively, and the total strain energy stored in the Q interior struts can be determined using Equation (28).

Then, the strain energy density function u in the unit cell with P boundary struts and Q interior struts can be obtained from Equations (28), (29) and (40). There are $6(M + B)$ unknowns contained in u , which include the $6M$ displacement and rotation components at the M interior nodes ($\mathbf{u}_m, \theta_m; m \in \{1, 2, \dots, M\}$) and the $6B$ periodic parts of the displacement and rotation components at the boundary nodes belonging to the B periodic pairs ($\mathbf{u}_n^*, \theta_n^*; n \in \{1, 2, \dots, B\}$). Accordingly, an equal number of equations are required to determine the unknown kinematic variables involved in the strain energy density function u . The $6B$ unknown periodic parts of the displacement and rotation components at the boundary nodes can be obtained by enforcing the anti-periodicity conditions of forces and moments for each periodic pair given in Equation (36). In addition, the $6M$ displacement and rotation components at the M interior nodes can be identified by imposing the force and moment equilibrium at those nodes according to Equation (31). Using these determined displacement and rotation components in Equation (29) will give the final expression of u , which can be used in Equation (32) to find the effective stiffness tensor $\bar{\mathbf{C}}$.

3. Case Studies

In this section, 2-D and 3-D cellular materials with and without periodicity constraints are homogenized by applying the generalized strain energy-based method proposed in Section 2. The mathematical formulation here is facilitated by using symbolic operations in MATLAB. For simplicity, in all cases considered here, struts are taken to be Bernoulli-Euler beams with uniform circular cross sections whose stiffness constants are given in Equation (4).

3.1. 2-D Cases

3.1.1. 2-D Homogenization without Periodicity Constraints

Consider a 2-D cellular material shown in Figure 4, which is asymmetric. The unit cell is composed of three struts with equal length L (i.e., $L^{(1)} = L^{(2)} = L^{(3)} = L$). The stiffness constants of each strut are given by

$$k_a^{(1)} = k_a^{(2)} = k_a^{(3)} = k_a, \quad k_s^{(1)} = k_s^{(2)} = k_s^{(3)} = k_s, \quad k_b^{(1)} = k_b^{(2)} = k_b^{(3)} = k_b, \quad (41)$$

where k_a , k_s and k_b are listed in Equation (4). The area of the unit cell is

$$A_{uc} = 2L^2. \quad (42)$$

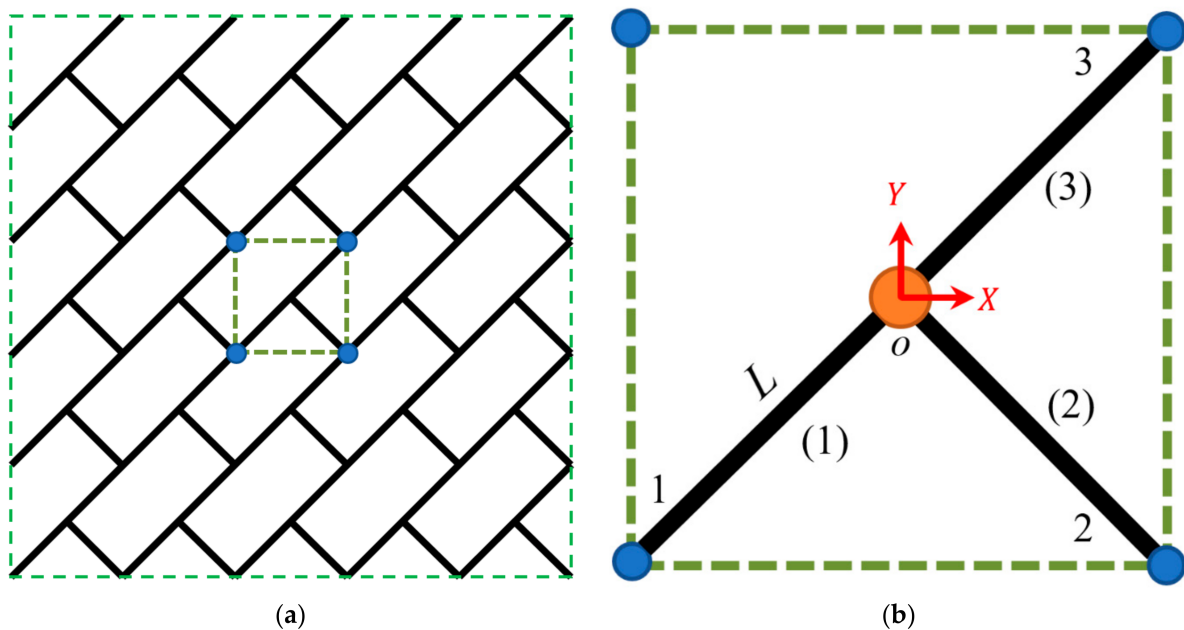


Figure 4. 2-D asymmetric cellular material: (a) microstructure; (b) unit cell.

The coordinate transformation tensor for each of the three struts with respect to the global coordinate system $\{X, Y, Z\}$ is given by

$$\mathbf{Q}^{(1)} = \begin{bmatrix} \frac{-1}{\sqrt{2}} & \frac{-1}{\sqrt{2}} & 0 \\ \frac{1}{\sqrt{2}} & \frac{-1}{\sqrt{2}} & 0 \\ 0 & 0 & 1 \end{bmatrix}, \quad \mathbf{Q}^{(2)} = \begin{bmatrix} \frac{1}{\sqrt{2}} & \frac{-1}{\sqrt{2}} & 0 \\ \frac{1}{\sqrt{2}} & \frac{1}{\sqrt{2}} & 0 \\ 0 & 0 & 1 \end{bmatrix}, \quad \mathbf{Q}^{(3)} = \begin{bmatrix} \frac{1}{\sqrt{2}} & \frac{1}{\sqrt{2}} & 0 \\ \frac{-1}{\sqrt{2}} & \frac{1}{\sqrt{2}} & 0 \\ 0 & 0 & 1 \end{bmatrix}. \quad (43)$$

In addition, the position vector of each boundary node with respect to the origin o (the center of the unit cell; an interior node) reads

$$\mathbf{x}_1 = \frac{-L}{\sqrt{2}} \{ 1 \ 1 \ 0 \}^T, \quad \mathbf{x}_2 = \frac{L}{\sqrt{2}} \{ 1 \ -1 \ 0 \}^T, \quad \mathbf{x}_3 = \frac{L}{\sqrt{2}} \{ 1 \ 1 \ 0 \}^T. \quad (44)$$

Substituting Equations (18) and (44) into Equation (22) gives the boundary conditions at the three boundary nodes as

$$\begin{Bmatrix} u_{X1} \\ u_{Y1} \end{Bmatrix} = -\frac{\sqrt{2}L}{2} \begin{Bmatrix} \bar{\varepsilon}_{XX} + \bar{\varepsilon}_{XY} \\ \bar{\varepsilon}_{XY} + \bar{\varepsilon}_{YY} \end{Bmatrix}, \quad \begin{Bmatrix} u_{X2} \\ u_{Y2} \end{Bmatrix} = \frac{\sqrt{2}L}{2} \begin{Bmatrix} \bar{\varepsilon}_{XX} - \bar{\varepsilon}_{XY} \\ \bar{\varepsilon}_{XY} - \bar{\varepsilon}_{YY} \end{Bmatrix}, \quad \begin{Bmatrix} u_{X3} \\ u_{Y3} \end{Bmatrix} = \frac{\sqrt{2}L}{2} \begin{Bmatrix} \bar{\varepsilon}_{XX} + \bar{\varepsilon}_{XY} \\ \bar{\varepsilon}_{XY} + \bar{\varepsilon}_{YY} \end{Bmatrix}, \quad (45)$$

$$M_{Z1} = 0, \quad M_{Z2} = 0, \quad M_{Z3} = 0. \quad (46)$$

Using Equations (1), (2), (7), (9), (13) and (43) in Equation (12) yields the force vector for each strut as

$$\begin{Bmatrix} F_{X0} \\ F_{Y0} \\ M_{Z0} \\ F_{X1} \\ F_{Y1} \\ M_{Z1} \end{Bmatrix} = \begin{Bmatrix} \left(\frac{k_a}{2} + \frac{k_s}{2}\right) \left(\frac{L\bar{\varepsilon}_{XX}}{\sqrt{2}} + \frac{L\bar{\varepsilon}_{XY}}{\sqrt{2}} + u_{X0}\right) + \left(\frac{k_a}{2} - \frac{k_s}{2}\right) \left(\frac{L\bar{\varepsilon}_{XY}}{\sqrt{2}} + \frac{L\bar{\varepsilon}_{YY}}{\sqrt{2}} + u_{Y0}\right) + \frac{Lk_s}{2\sqrt{2}}(\theta_{Z0} + \theta_{Z1}) \\ \left(\frac{k_a}{2} + \frac{k_s}{2}\right) \left(\frac{L\bar{\varepsilon}_{XY}}{\sqrt{2}} + \frac{L\bar{\varepsilon}_{YY}}{\sqrt{2}} + u_{Y0}\right) + \left(\frac{k_a}{2} - \frac{k_s}{2}\right) \left(\frac{L\bar{\varepsilon}_{XX}}{\sqrt{2}} + \frac{L\bar{\varepsilon}_{XY}}{\sqrt{2}} + u_{X0}\right) - \frac{Lk_s}{2\sqrt{2}}(\theta_{Z0} + \theta_{Z1}) \\ k_b\theta_{Z0} - \left(k_b - \frac{L^2k_s}{2}\right)\theta_{Z1} + \frac{L^2k_s}{4}(\bar{\varepsilon}_{XX} - \bar{\varepsilon}_{YY}) + \frac{Lk_s}{2\sqrt{2}}(u_{X0} - u_{Y0}) \\ -\left(\frac{k_a}{2} + \frac{k_s}{2}\right) \left(\frac{L\bar{\varepsilon}_{XX}}{\sqrt{2}} + \frac{L\bar{\varepsilon}_{XY}}{\sqrt{2}} + u_{X0}\right) - \left(\frac{k_a}{2} - \frac{k_s}{2}\right) \left(\frac{L\bar{\varepsilon}_{XY}}{\sqrt{2}} + \frac{L\bar{\varepsilon}_{YY}}{\sqrt{2}} + u_{Y0}\right) - \frac{Lk_s}{2\sqrt{2}}(\theta_{Z0} + \theta_{Z1}) \\ -\left(\frac{k_a}{2} + \frac{k_s}{2}\right) \left(\frac{L\bar{\varepsilon}_{XY}}{\sqrt{2}} + \frac{L\bar{\varepsilon}_{YY}}{\sqrt{2}} + u_{Y0}\right) - \left(\frac{k_a}{2} - \frac{k_s}{2}\right) \left(\frac{L\bar{\varepsilon}_{XX}}{\sqrt{2}} + \frac{L\bar{\varepsilon}_{XY}}{\sqrt{2}} + u_{X0}\right) + \frac{Lk_s}{2\sqrt{2}}(\theta_{Z0} + \theta_{Z1}) \\ k_b\theta_{Z1} - \left(k_b - \frac{L^2k_s}{2}\right)\theta_{Z0} + \frac{L^2k_s}{4}(\bar{\varepsilon}_{XX} - \bar{\varepsilon}_{YY}) + \frac{Lk_s}{2\sqrt{2}}(u_{X0} - u_{Y0}) \end{Bmatrix}, \quad (47)$$

$$\begin{Bmatrix} F_{X0} \\ F_{Y0} \\ M_{Z0} \\ F_{X2} \\ F_{Y2} \\ M_{Z2} \end{Bmatrix} = \begin{Bmatrix} \left(\frac{k_a}{2} + \frac{k_s}{2}\right) \left(\frac{L\bar{\varepsilon}_{XY}}{\sqrt{2}} - \frac{L\bar{\varepsilon}_{XX}}{\sqrt{2}} + u_{X0}\right) - \left(\frac{k_a}{2} - \frac{k_s}{2}\right) \left(\frac{L\bar{\varepsilon}_{YY}}{\sqrt{2}} - \frac{L\bar{\varepsilon}_{XY}}{\sqrt{2}} + u_{Y0}\right) + \frac{Lk_s}{2\sqrt{2}}(\theta_{Z0} + \theta_{Z2}) \\ \left(\frac{k_a}{2} + \frac{k_s}{2}\right) \left(\frac{L\bar{\varepsilon}_{YY}}{\sqrt{2}} - \frac{L\bar{\varepsilon}_{XY}}{\sqrt{2}} + u_{Y0}\right) + \left(\frac{k_a}{2} - \frac{k_s}{2}\right) \left(\frac{L\bar{\varepsilon}_{XX}}{\sqrt{2}} - \frac{L\bar{\varepsilon}_{XY}}{\sqrt{2}} - u_{X0}\right) + \frac{Lk_s}{2\sqrt{2}}(\theta_{Z0} + \theta_{Z2}) \\ k_b\theta_{Z0} - \left(k_b - \frac{L^2k_s}{2}\right)\theta_{Z2} - \frac{L^2k_s}{4}(\bar{\varepsilon}_{XX} - \bar{\varepsilon}_{YY}) + \frac{Lk_s}{2\sqrt{2}}(u_{X0} + u_{Y0}) \\ -\left(\frac{k_a}{2} + \frac{k_s}{2}\right) \left(\frac{L\bar{\varepsilon}_{XY}}{\sqrt{2}} - \frac{L\bar{\varepsilon}_{XX}}{\sqrt{2}} + u_{X0}\right) + \left(\frac{k_a}{2} - \frac{k_s}{2}\right) \left(\frac{L\bar{\varepsilon}_{YY}}{\sqrt{2}} - \frac{L\bar{\varepsilon}_{XY}}{\sqrt{2}} + u_{Y0}\right) - \frac{Lk_s}{2\sqrt{2}}(\theta_{Z0} + \theta_{Z2}) \\ -\left(\frac{k_a}{2} + \frac{k_s}{2}\right) \left(\frac{L\bar{\varepsilon}_{YY}}{\sqrt{2}} - \frac{L\bar{\varepsilon}_{XY}}{\sqrt{2}} + u_{Y0}\right) - \left(\frac{k_a}{2} - \frac{k_s}{2}\right) \left(\frac{L\bar{\varepsilon}_{XX}}{\sqrt{2}} - \frac{L\bar{\varepsilon}_{XY}}{\sqrt{2}} - u_{X0}\right) - \frac{Lk_s}{2\sqrt{2}}(\theta_{Z0} + \theta_{Z2}) \\ k_b\theta_{Z2} - \left(k_b - \frac{L^2k_s}{2}\right)\theta_{Z0} - \frac{L^2k_s}{4}(\bar{\varepsilon}_{XX} - \bar{\varepsilon}_{YY}) + \frac{Lk_s}{2\sqrt{2}}(u_{X0} + u_{Y0}) \end{Bmatrix}, \quad (48)$$

$$\begin{Bmatrix} F_{X0} \\ F_{Y0} \\ M_{Z0} \\ F_{X3} \\ F_{Y3} \\ M_{Z3} \end{Bmatrix} = \begin{Bmatrix} \left(\frac{k_a}{2} + \frac{k_s}{2}\right) \left(-\frac{L\bar{\varepsilon}_{XY}}{\sqrt{2}} - \frac{L\bar{\varepsilon}_{XX}}{\sqrt{2}} + u_{X0}\right) + \left(\frac{k_a}{2} - \frac{k_s}{2}\right) \left(-\frac{L\bar{\varepsilon}_{YY}}{\sqrt{2}} - \frac{L\bar{\varepsilon}_{XY}}{\sqrt{2}} + u_{Y0}\right) - \frac{Lk_s}{2\sqrt{2}}(\theta_{Z0} + \theta_{Z3}) \\ \left(\frac{k_a}{2} + \frac{k_s}{2}\right) \left(-\frac{L\bar{\varepsilon}_{YY}}{\sqrt{2}} - \frac{L\bar{\varepsilon}_{XY}}{\sqrt{2}} + u_{Y0}\right) + \left(\frac{k_a}{2} - \frac{k_s}{2}\right) \left(-\frac{L\bar{\varepsilon}_{XX}}{\sqrt{2}} - \frac{L\bar{\varepsilon}_{XY}}{\sqrt{2}} + u_{X0}\right) + \frac{Lk_s}{2\sqrt{2}}(\theta_{Z0} + \theta_{Z3}) \\ k_b\theta_{Z0} - \left(k_b - \frac{L^2k_s}{2}\right)\theta_{Z3} + \frac{L^2k_s}{4}(\bar{\varepsilon}_{XX} - \bar{\varepsilon}_{YY}) - \frac{Lk_s}{2\sqrt{2}}(u_{X0} - u_{Y0}) \\ \left(\frac{k_a}{2} + \frac{k_s}{2}\right) \left(\frac{L\bar{\varepsilon}_{XY}}{\sqrt{2}} + \frac{L\bar{\varepsilon}_{XX}}{\sqrt{2}} - u_{X0}\right) + \left(\frac{k_a}{2} - \frac{k_s}{2}\right) \left(\frac{L\bar{\varepsilon}_{YY}}{\sqrt{2}} + \frac{L\bar{\varepsilon}_{XY}}{\sqrt{2}} - u_{Y0}\right) + \frac{Lk_s}{2\sqrt{2}}(\theta_{Z0} + \theta_{Z3}) \\ \left(\frac{k_a}{2} + \frac{k_s}{2}\right) \left(\frac{L\bar{\varepsilon}_{YY}}{\sqrt{2}} + \frac{L\bar{\varepsilon}_{XY}}{\sqrt{2}} - u_{Y0}\right) + \left(\frac{k_a}{2} - \frac{k_s}{2}\right) \left(\frac{L\bar{\varepsilon}_{XX}}{\sqrt{2}} + \frac{L\bar{\varepsilon}_{XY}}{\sqrt{2}} - u_{X0}\right) - \frac{Lk_s}{2\sqrt{2}}(\theta_{Z0} + \theta_{Z3}) \\ k_b\theta_{Z3} - \left(k_b - \frac{L^2k_s}{2}\right)\theta_{Z0} + \frac{L^2k_s}{4}(\bar{\varepsilon}_{XX} - \bar{\varepsilon}_{YY}) - \frac{Lk_s}{2\sqrt{2}}(u_{X0} - u_{Y0}) \end{Bmatrix}. \quad (49)$$

Substituting Equations (47)–(49) into Equation (46) or (30), which gives the moment equilibrium equations at the three boundary nodes in Figure 4b, leads to the rotation components at the three boundary nodes as

$$\begin{aligned} \theta_{Z1} &= \theta_{Z0} - \frac{Lk_s(L\bar{\varepsilon}_{XX} - L\bar{\varepsilon}_{YY} + 2L\theta_{Z0} + \sqrt{2}u_{X0} - \sqrt{2}u_{Y0})}{4k_b}, \\ \theta_{Z2} &= \theta_{Z0} - \frac{Lk_s(L\bar{\varepsilon}_{YY} - L\bar{\varepsilon}_{XX} + 2L\theta_{Z0} + \sqrt{2}u_{X0} + \sqrt{2}u_{Y0})}{4k_b}, \\ \theta_{Z3} &= \theta_{Z0} - \frac{Lk_s(L\bar{\varepsilon}_{XX} - L\bar{\varepsilon}_{YY} + 2L\theta_{Z0} - \sqrt{2}u_{X0} + \sqrt{2}u_{Y0})}{4k_b}. \end{aligned} \quad (50)$$

Using Equation (47)–(49) and (50) in Equation (31), the force and moment equilibrium equations at the interior node o , results in

$$\begin{bmatrix} \frac{3k_a}{2} + \frac{3k_s}{2} - \frac{3L^2k_s^2}{8k_b} & \frac{k_a}{2} - \frac{k_s}{2} + \frac{L^2k_s^2}{8k_b} & \frac{\sqrt{2}Lk_s}{2} - \frac{\sqrt{2}L^3k_s^2}{8k_b} \\ \frac{k_a}{2} - \frac{k_s}{2} + \frac{L^2k_s^2}{8k_b} & \frac{3k_a}{2} + \frac{3k_s}{2} - \frac{3L^2k_s^2}{8k_b} & \frac{\sqrt{2}Lk_s}{2} - \frac{\sqrt{2}L^3k_s^2}{8k_b} \\ \frac{\sqrt{2}Lk_s}{2} - \frac{\sqrt{2}L^3k_s^2}{8k_b} & \frac{\sqrt{2}Lk_s}{2} - \frac{\sqrt{2}L^3k_s^2}{8k_b} & 3L^2k_s - \frac{3L^4k_s^2}{4k_b} \end{bmatrix} \begin{Bmatrix} u_{X0} \\ u_{Y0} \\ \theta_{Z0} \end{Bmatrix} = \begin{Bmatrix} B_1 \\ B_2 \\ B_3 \end{Bmatrix}, \quad (51)$$

where

$$\begin{aligned} B_1 &= \frac{\sqrt{2}L(k_a\bar{\epsilon}_{XX} - 2k_a\bar{\epsilon}_{XY} + k_a\bar{\epsilon}_{YY} + k_s\bar{\epsilon}_{XX} - k_s\bar{\epsilon}_{YY})}{4} - \frac{\sqrt{2}L^3k_s^2(\bar{\epsilon}_{XX} - \bar{\epsilon}_{YY})}{16k_b}, \\ B_2 &= -\frac{\sqrt{2}L(k_a\bar{\epsilon}_{XX} - 2k_a\bar{\epsilon}_{XY} + k_a\bar{\epsilon}_{YY} - k_s\bar{\epsilon}_{XX} + k_s\bar{\epsilon}_{YY})}{4} - \frac{\sqrt{2}L^3k_s^2(\bar{\epsilon}_{XX} - \bar{\epsilon}_{YY})}{16k_b}, \\ B_3 &= -\frac{L^2k_s(\bar{\epsilon}_{XX} - \bar{\epsilon}_{YY})(4k_b - L^2k_s)}{8k_b}. \end{aligned} \quad (52)$$

Upon solving the system of three equations in Equation (51), the displacement and rotation components at the interior node can be obtained as

$$\begin{aligned} u_{X0} &= \frac{\sqrt{2}Lk_s(4k_b - L^2k_s)}{2(12k_ak_b + 4k_bk_s - L^2k_s^2)}(\bar{\epsilon}_{XX} - \bar{\epsilon}_{YY}) + \frac{\sqrt{2}Lk_ak_b}{2(2k_ak_b + 4k_bk_s - L^2k_s^2)}(\bar{\epsilon}_{XX} - 2\bar{\epsilon}_{XY} + \bar{\epsilon}_{YY}), \\ u_{Y0} &= \frac{\sqrt{2}Lk_s(4k_b - L^2k_s)}{2(12k_ak_b + 4k_bk_s - L^2k_s^2)}(\bar{\epsilon}_{XX} - \bar{\epsilon}_{YY}) - \frac{\sqrt{2}Lk_ak_b}{2(2k_ak_b + 4k_bk_s - L^2k_s^2)}(\bar{\epsilon}_{XX} - 2\bar{\epsilon}_{XY} + \bar{\epsilon}_{YY}), \\ u_{Z0} &= -\frac{4k_ak_b + 4k_bk_s - L^2k_s^2}{2(12k_ak_b + 4k_bk_s - L^2k_s^2)}(\bar{\epsilon}_{XX} - \bar{\epsilon}_{YY}). \end{aligned} \quad (53)$$

Substituting Equations (1), (2), (9), (15), (25), (41), (43), (45), (50) and (53) into Equation (29) gives the strain energy density function as

$$\begin{aligned} u &= \frac{11k_a}{16}(\bar{\epsilon}_{XX}^2 + \bar{\epsilon}_{YY}^2) + \frac{3k_a}{4}\bar{\epsilon}_{XY}^2 + \frac{k_a}{4}\bar{\epsilon}_{XY}(\bar{\epsilon}_{XX} + \bar{\epsilon}_{YY}) - \frac{5k_a}{8}\bar{\epsilon}_{XX}\bar{\epsilon}_{YY} \\ &\quad - \frac{6k_a^2k_b}{12k_ak_b + 4k_bk_s - L^2k_s^2}(\bar{\epsilon}_{XX} - \bar{\epsilon}_{YY})^2 - \frac{k_a^2k_b}{8(2k_ak_b + 4k_bk_s - L^2k_s^2)}(\bar{\epsilon}_{XX} - 2\bar{\epsilon}_{XY} + \bar{\epsilon}_{YY})^2. \end{aligned} \quad (54)$$

Clearly, Equation (54) does not contain any unknown kinematic variable.

It then follows from Equations (32) and (54) that the effective stiffness matrix $\bar{\mathbf{C}}$ for the 2-D cellular material can be obtained from the coefficient matrix of the following constitutive equations:

$$\begin{Bmatrix} \bar{\sigma}_{XX} \\ \bar{\sigma}_{YY} \\ \bar{\sigma}_{XY} \end{Bmatrix} = \begin{bmatrix} \chi_2 & \chi_3 & \chi_1 \\ \chi_3 & \chi_2 & \chi_1 \\ \chi_1 & \chi_1 & \chi_4 \end{bmatrix} \begin{Bmatrix} \bar{\epsilon}_{XX} \\ \bar{\epsilon}_{YY} \\ \bar{\epsilon}_{XY} \end{Bmatrix} = \bar{\mathbf{C}} \begin{Bmatrix} \bar{\epsilon}_{XX} \\ \bar{\epsilon}_{YY} \\ \bar{\epsilon}_{XY} \end{Bmatrix}, \quad (55)$$

where

$$\begin{aligned} \chi_1 &= \frac{k_a}{4} + \frac{k_a^2k_b}{2(2k_ak_b + 4k_bk_s - L^2k_s^2)}, \\ \chi_2 &= \frac{11k_a}{8} - \frac{k_a^2k_b}{4(2k_ak_b + 4k_bk_s - L^2k_s^2)} - \frac{12k_a^2k_b}{12k_ak_b + 4k_bk_s - L^2k_s^2}, \\ \chi_3 &= -\frac{5k_a}{8} + \frac{12k_a^2k_b}{12k_ak_b + 4k_bk_s - L^2k_s^2} - \frac{k_a^2k_b}{4(2k_ak_b + 4k_bk_s - L^2k_s^2)}, \\ \chi_4 &= \frac{3k_a}{2} - \frac{k_a^2k_b}{2k_ak_b + 4k_bk_s - L^2k_s^2}. \end{aligned} \quad (56)$$

Note that only one specific configuration shown in Figure 4 is considered in the 2-D case studies here. However, the inclination angle of struts in the 2-D asymmetric cellular material displayed in Figure 4a could be set as an adjustable variable, which would lead to the orientation dependence of the effective elastic properties upon using the current homogenization method. Such orientation dependence exhibited by 2-D cellular materials has been extensively studied (e.g., [20,25,47]).

3.1.1.1. 2-D Homogenization with Periodicity Constraints

In this sub-section, periodicity constraints are imposed on the unit cell shown in Figure 4b, which is further illustrated in Figure 5. It can be seen from Figure 5 that the three nodes on the boundary of the unit cell form one periodic pair (with $B = 1$ and $H = 3$).

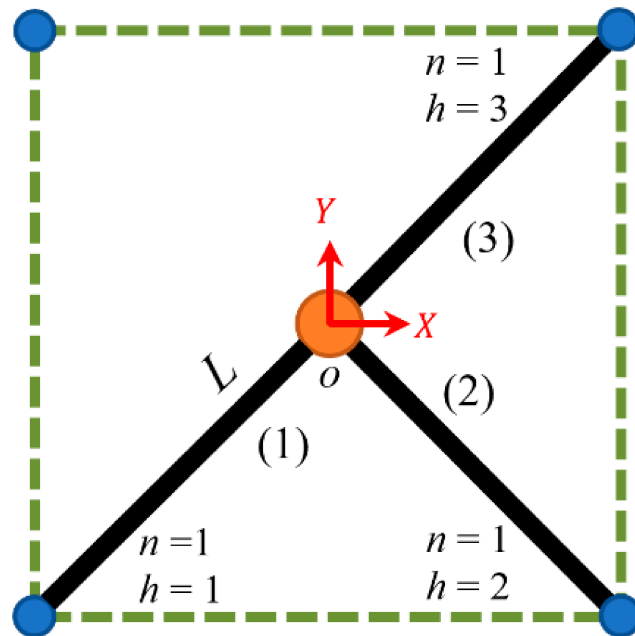


Figure 5. 2-D asymmetric unit cell with periodicity constraints.

Based on the conditions listed in Equations (35) and (36), the periodicity constraints for the unit cell shown in Figure 5 take the following form:

$$\begin{Bmatrix} u_{X1}^* \\ u_{Y1}^* \\ \theta_{Z1}^* \end{Bmatrix} = \begin{Bmatrix} u_{X2}^* \\ u_{Y2}^* \\ \theta_{Z2}^* \end{Bmatrix} = \begin{Bmatrix} u_{X3}^* \\ u_{Y3}^* \\ \theta_{Z3}^* \end{Bmatrix} = \begin{Bmatrix} u_X^* \\ u_Y^* \\ \theta_Z^* \end{Bmatrix}, \quad \begin{Bmatrix} F_{X1} + F_{X2} + F_{X3} \\ F_{Y1} + F_{Y2} + F_{Y3} \\ M_{Z1} + M_{Z2} + M_{Z3} \end{Bmatrix} = \begin{Bmatrix} 0 \\ 0 \\ 0 \end{Bmatrix}. \quad (57)$$

Substituting Equations (45) and (57) (the first set) into Equation (37) yields the periodic boundary conditions at the three boundary nodes as

$$\begin{Bmatrix} u_{X1} \\ u_{Y1} \\ \theta_{Z1} \end{Bmatrix} = -\frac{\sqrt{2}L}{2} \begin{Bmatrix} \bar{\epsilon}_{XX} + \bar{\epsilon}_{XY} \\ \bar{\epsilon}_{XY} + \bar{\epsilon}_{YY} \\ 0 \end{Bmatrix} + \begin{Bmatrix} u_X^* \\ u_Y^* \\ \theta_Z^* \end{Bmatrix}, \quad \begin{Bmatrix} u_{X2} \\ u_{Y2} \\ \theta_{Z2} \end{Bmatrix} = \frac{\sqrt{2}L}{2} \begin{Bmatrix} \bar{\epsilon}_{XX} - \bar{\epsilon}_{XY} \\ \bar{\epsilon}_{XY} - \bar{\epsilon}_{YY} \\ 0 \end{Bmatrix} + \begin{Bmatrix} u_X^* \\ u_Y^* \\ \theta_Z^* \end{Bmatrix}, \quad (58)$$

$$\begin{Bmatrix} u_{X3} \\ u_{Y3} \\ \theta_{Z3} \end{Bmatrix} = \frac{\sqrt{2}L}{2} \begin{Bmatrix} \bar{\epsilon}_{XX} + \bar{\epsilon}_{XY} \\ \bar{\epsilon}_{XY} + \bar{\epsilon}_{YY} \\ 0 \end{Bmatrix} + \begin{Bmatrix} u_X^* \\ u_Y^* \\ \theta_Z^* \end{Bmatrix}.$$

Using Equations (1), (2), (7), (9), (13), (43) and (58) in Equation (12) gives the nodal force vector for each of the three struts as

$$\begin{Bmatrix} F_{X0} \\ F_{Y0} \\ M_{Z0} \\ F_{X1} \\ F_{Y1} \\ M_{Z1} \end{Bmatrix} = \begin{Bmatrix} \frac{1}{2}(k_a + k_s) \left(\frac{L\bar{\epsilon}_{XX}}{\sqrt{2}} + \frac{L\bar{\epsilon}_{XY}}{\sqrt{2}} + u_{X0} - u_X^* \right) + \frac{1}{2}(k_a - k_s) \left(\frac{L\bar{\epsilon}_{XY}}{\sqrt{2}} + \frac{L\bar{\epsilon}_{YY}}{\sqrt{2}} + u_{Y0} - u_Y^* \right) + \frac{Lk_s}{2\sqrt{2}} (\theta_{Z0} + \theta_Z^*) \\ \frac{1}{2}(k_a + k_s) \left(\frac{L\bar{\epsilon}_{XY}}{\sqrt{2}} + \frac{L\bar{\epsilon}_{YY}}{\sqrt{2}} + u_{Y0} - u_Y^* \right) + \frac{1}{2}(k_a - k_s) \left(\frac{L\bar{\epsilon}_{XX}}{\sqrt{2}} + \frac{L\bar{\epsilon}_{XY}}{\sqrt{2}} + u_{X0} - u_X^* \right) - \frac{Lk_s}{2\sqrt{2}} (\theta_{Z0} + \theta_Z^*) \\ k_b \theta_{Z0} - \left(k_b - \frac{L^2 k_s}{2} \right) \theta_Z^* + \frac{L^2 k_s}{4} (\bar{\epsilon}_{XX} - \bar{\epsilon}_{YY}) + \frac{Lk_s}{2\sqrt{2}} (u_{X0} - u_X^* - u_{Y0} + u_Y^*) \\ -\frac{1}{2}(k_a + k_s) \left(\frac{L\bar{\epsilon}_{XX}}{\sqrt{2}} + \frac{L\bar{\epsilon}_{XY}}{\sqrt{2}} + u_{X0} - u_X^* \right) - \frac{1}{2}(k_a - k_s) \left(\frac{L\bar{\epsilon}_{XY}}{\sqrt{2}} + \frac{L\bar{\epsilon}_{YY}}{\sqrt{2}} + u_{Y0} - u_Y^* \right) - \frac{Lk_s}{2\sqrt{2}} (\theta_{Z0} + \theta_Z^*) \\ -\frac{1}{2}(k_a + k_s) \left(\frac{L\bar{\epsilon}_{XY}}{\sqrt{2}} + \frac{L\bar{\epsilon}_{YY}}{\sqrt{2}} + u_{Y0} - u_Y^* \right) - \frac{1}{2}(k_a - k_s) \left(\frac{L\bar{\epsilon}_{XX}}{\sqrt{2}} + \frac{L\bar{\epsilon}_{XY}}{\sqrt{2}} + u_{X0} - u_X^* \right) + \frac{Lk_s}{2\sqrt{2}} (\theta_{Z0} + \theta_Z^*) \\ k_b \theta_Z^* - \left(k_b - \frac{L^2 k_s}{2} \right) \theta_{Z0} + \frac{L^2 k_s}{4} (\bar{\epsilon}_{XX} - \bar{\epsilon}_{YY}) + \frac{Lk_s}{2\sqrt{2}} (u_{X0} - u_X^* - u_{Y0} + u_Y^*) \end{Bmatrix} \quad (59)$$

$$\begin{Bmatrix} F_{X0} \\ F_{Y0} \\ M_{Z0} \\ F_{X2} \\ F_{Y2} \\ M_{Z2} \end{Bmatrix} = \begin{Bmatrix} \frac{1}{2}(k_a + k_s) \left(-\frac{L\bar{\epsilon}_{XX}}{\sqrt{2}} + \frac{L\bar{\epsilon}_{XY}}{\sqrt{2}} + u_{X0} - u_X^* \right) - \frac{1}{2}(k_a - k_s) \left(-\frac{L\bar{\epsilon}_{XY}}{\sqrt{2}} + \frac{L\bar{\epsilon}_{YY}}{\sqrt{2}} + u_{Y0} - u_Y^* \right) + \frac{Lk_s}{2\sqrt{2}} (\theta_{Z0} + \theta_Z^*) \\ \frac{1}{2}(k_a + k_s) \left(-\frac{L\bar{\epsilon}_{XY}}{\sqrt{2}} + \frac{L\bar{\epsilon}_{YY}}{\sqrt{2}} + u_{Y0} - u_Y^* \right) + \frac{1}{2}(k_a - k_s) \left(\frac{L\bar{\epsilon}_{XX}}{\sqrt{2}} - \frac{L\bar{\epsilon}_{XY}}{\sqrt{2}} - u_{X0} + u_X^* \right) + \frac{Lk_s}{2\sqrt{2}} (\theta_{Z0} + \theta_Z^*) \\ k_b \theta_{Z0} - \left(k_b - \frac{L^2 k_s}{2} \right) \theta_Z^* - \frac{L^2 k_s}{4} (\bar{\epsilon}_{XX} - \bar{\epsilon}_{YY}) + \frac{Lk_s}{2\sqrt{2}} (u_{X0} - u_X^* + u_{Y0} - u_Y^*) \\ -\frac{1}{2}(k_a + k_s) \left(-\frac{L\bar{\epsilon}_{XX}}{\sqrt{2}} + \frac{L\bar{\epsilon}_{XY}}{\sqrt{2}} + u_{X0} - u_X^* \right) + \frac{1}{2}(k_a - k_s) \left(-\frac{L\bar{\epsilon}_{XY}}{\sqrt{2}} + \frac{L\bar{\epsilon}_{YY}}{\sqrt{2}} + u_{Y0} - u_Y^* \right) - \frac{Lk_s}{2\sqrt{2}} (\theta_{Z0} + \theta_Z^*) \\ -\frac{1}{2}(k_a + k_s) \left(-\frac{L\bar{\epsilon}_{XY}}{\sqrt{2}} + \frac{L\bar{\epsilon}_{YY}}{\sqrt{2}} + u_{Y0} - u_Y^* \right) - \left(\frac{k_a}{2} - \frac{k_s}{2} \right) \left(\frac{L\bar{\epsilon}_{XX}}{\sqrt{2}} - \frac{L\bar{\epsilon}_{XY}}{\sqrt{2}} - u_{X0} + u_X^* \right) - \frac{Lk_s}{2\sqrt{2}} (\theta_{Z0} + \theta_Z^*) \\ k_b \theta_Z^* - \left(k_b - \frac{L^2 k_s}{2} \right) \theta_{Z0} - \frac{L^2 k_s}{4} (\bar{\epsilon}_{XX} - \bar{\epsilon}_{YY}) + \frac{Lk_s}{2\sqrt{2}} (u_{X0} - u_X^* + u_{Y0} - u_Y^*) \end{Bmatrix} \quad (60)$$

$$\begin{Bmatrix} F_{X0} \\ F_{Y0} \\ M_{Z0} \\ F_{X3} \\ F_{Y3} \\ M_{Z3} \end{Bmatrix} = \begin{Bmatrix} \frac{1}{2}(k_a + k_s) \left(-\frac{L\bar{\epsilon}_{XX}}{\sqrt{2}} - \frac{L\bar{\epsilon}_{XY}}{\sqrt{2}} + u_{X0} - u_X^* \right) + \frac{1}{2}(k_a - k_s) \left(-\frac{L\bar{\epsilon}_{XY}}{\sqrt{2}} - \frac{L\bar{\epsilon}_{YY}}{\sqrt{2}} + u_{Y0} - u_Y^* \right) - \frac{Lk_s}{2\sqrt{2}} (\theta_{Z0} + \theta_Z^*) \\ \frac{1}{2}(k_a + k_s) \left(-\frac{L\bar{\epsilon}_{XY}}{\sqrt{2}} - \frac{L\bar{\epsilon}_{YY}}{\sqrt{2}} + u_{Y0} - u_Y^* \right) + \frac{1}{2}(k_a - k_s) \left(-\frac{L\bar{\epsilon}_{XX}}{\sqrt{2}} - \frac{L\bar{\epsilon}_{XY}}{\sqrt{2}} + u_{X0} - u_X^* \right) + \frac{Lk_s}{2\sqrt{2}} (\theta_{Z0} + \theta_Z^*) \\ k_b \theta_{Z0} - \left(k_b - \frac{L^2 k_s}{2} \right) \theta_Z^* + \frac{L^2 k_s}{4} (\bar{\epsilon}_{XX} - \bar{\epsilon}_{YY}) - \frac{Lk_s}{2\sqrt{2}} (u_{X0} - u_X^* - u_{Y0} + u_Y^*) \\ \frac{1}{2}(k_a + k_s) \left(\frac{L\bar{\epsilon}_{XX}}{\sqrt{2}} + \frac{L\bar{\epsilon}_{XY}}{\sqrt{2}} - u_{X0} + u_X^* \right) + \frac{1}{2}(k_a - k_s) \left(\frac{L\bar{\epsilon}_{XY}}{\sqrt{2}} + \frac{L\bar{\epsilon}_{YY}}{\sqrt{2}} - u_{Y0} + u_Y^* \right) + \frac{Lk_s}{2\sqrt{2}} (\theta_{Z0} + \theta_Z^*) \\ \frac{1}{2}(k_a + k_s) \left(\frac{L\bar{\epsilon}_{XY}}{\sqrt{2}} + \frac{L\bar{\epsilon}_{YY}}{\sqrt{2}} - u_{Y0} + u_Y^* \right) + \frac{1}{2}(k_a - k_s) \left(\frac{L\bar{\epsilon}_{XX}}{\sqrt{2}} + \frac{L\bar{\epsilon}_{XY}}{\sqrt{2}} - u_{X0} + u_X^* \right) - \frac{Lk_s}{2\sqrt{2}} (\theta_{Z0} + \theta_Z^*) \\ k_b \theta_Z^* - \left(k_b - \frac{L^2 k_s}{2} \right) \theta_{Z0} + \frac{L^2 k_s}{4} (\bar{\epsilon}_{XX} - \bar{\epsilon}_{YY}) - \frac{Lk_s}{2\sqrt{2}} (u_{X0} - u_X^* - u_{Y0} + u_Y^*) \end{Bmatrix} \quad (61)$$

Substituting Equations (59)–(61) into Equation (57) (the second set) results in

$$\begin{bmatrix} \frac{3k_a}{2} + \frac{3k_s}{2} & \frac{k_a}{2} - \frac{k_s}{2} & -\frac{\sqrt{2}Lk_s}{4} \\ \frac{k_a}{2} - \frac{k_s}{2} & \frac{3k_a}{2} + \frac{3k_s}{2} & -\frac{\sqrt{2}Lk_s}{4} \\ -\frac{\sqrt{2}Lk_s}{4} & -\frac{\sqrt{2}Lk_s}{4} & 3k_b \end{bmatrix} \begin{Bmatrix} u_X^* \\ u_Y^* \\ \theta_Z^* \end{Bmatrix} = \begin{Bmatrix} B_1 \\ B_2 \\ B_3 \end{Bmatrix}, \quad (62)$$

where

$$\begin{aligned} B_1 &= -\frac{\sqrt{2}L}{4} (k_a + k_s) (\bar{\epsilon}_{XX} - \bar{\epsilon}_{XY}) + \frac{\sqrt{2}L}{4} (k_a - k_s) (\bar{\epsilon}_{XY} - \bar{\epsilon}_{YY}) \\ &\quad + \frac{3}{2} (k_a + k_s) u_{X0} + \frac{1}{2} (k_a - k_s) u_{Y0} + \frac{\sqrt{2}L}{4} k_s \theta_{Z0}, \\ B_2 &= \frac{\sqrt{2}L}{4} (k_a - k_s) (\bar{\epsilon}_{XX} - \bar{\epsilon}_{XY}) - \frac{\sqrt{2}L}{4} (k_a + k_s) (\bar{\epsilon}_{XY} - \bar{\epsilon}_{YY}) \\ &\quad + \frac{1}{2} (k_a - k_s) u_{X0} + \frac{3}{2} (k_a + k_s) u_{Y0} + \frac{\sqrt{2}Lk_s}{4} \theta_{Z0}, \\ B_3 &= -\frac{L^2 k_s}{4} (\bar{\epsilon}_{XX} - \bar{\epsilon}_{YY}) - \frac{\sqrt{2}Lk_s}{4} u_{X0} - \frac{\sqrt{2}Lk_s}{4} u_{Y0} + 3 \left(k_b - \frac{L^2 k_s}{2} \right) \theta_{Z0}. \end{aligned} \quad (63)$$

Upon solving Equation (62), the periodic parts of the displacement and rotation components at the three boundary nodes are obtained as

$$\begin{aligned}
 u_X^* &= u_{Xo} - \frac{k_a L}{2\sqrt{2}(k_a+2k_s)} (\bar{\epsilon}_{XX} - 2\bar{\epsilon}_{XY} + \bar{\epsilon}_{YY}) \\
 &\quad - \frac{Lk_s [(12k_b+L^2k_s)(\bar{\epsilon}_{XX}-\bar{\epsilon}_{YY})-6(4k_b-L^2k_s)\theta_{Zo}]}{2\sqrt{2}(24k_a k_b+12k_b k_s-L^2k_s^2)}, \\
 u_Y^* &= u_{Yo} + \frac{k_a L}{2\sqrt{2}(k_a+2k_s)} (\bar{\epsilon}_{XX} - 2\bar{\epsilon}_{XY} + \bar{\epsilon}_{YY}) \\
 &\quad - \frac{Lk_s [(12k_b+L^2k_s)(\bar{\epsilon}_{XX}-\bar{\epsilon}_{YY})-6(4k_b-L^2k_s)\theta_{Zo}]}{2\sqrt{2}(24k_a k_b+12k_b k_s-L^2k_s^2)}, \\
 \theta_Z^* &= \theta_{Zo} - \frac{2L^2k_s [(k_a+k_s)(\bar{\epsilon}_{XX}-\bar{\epsilon}_{YY})+2(3k_a+k_s)\theta_{Zo}]}{24k_a k_b+12k_b k_s-L^2k_s^2}.
 \end{aligned}
 \tag{64}$$

Substituting Equations (59)–(61) and (64) into Equation (31) gives, from the equilibrium of the interior (central) node *o*,

$$\theta_{Zo} = -\frac{k_a + k_s}{2(3k_a + k_s)} (\bar{\epsilon}_{XX} - \bar{\epsilon}_{YY})
 \tag{65}$$

after setting $u_{Xo} = u_{Yo} = 0$ (i.e., no rigid-body displacement enforced at the central node *o*).

Using Equations (1), (2), (9), (15), (25), (41), (43), (58), (64) and (65) in Equation (29) yields the stain energy density function as

$$\begin{aligned}
 u &= \frac{k_a}{16} (11\bar{\epsilon}_{XX}^2 + 4\bar{\epsilon}_{XX}\bar{\epsilon}_{XY} - 10\bar{\epsilon}_{XX}\bar{\epsilon}_{YY} + 12\bar{\epsilon}_{XY}^2 + 4\bar{\epsilon}_{XY}\bar{\epsilon}_{YY} + 11\bar{\epsilon}_{YY}^2) \\
 &\quad - \frac{3k_a^2}{2(3k_a+k_s)} (\bar{\epsilon}_{XX} - \bar{\epsilon}_{YY})^2 - \frac{k_a^2}{16(k_a+2k_s)} (\bar{\epsilon}_{XX} - 2\bar{\epsilon}_{XY} + \bar{\epsilon}_{YY})^2,
 \end{aligned}
 \tag{66}$$

which does not involve any unknown kinematic variable.

Then, it follows from Equations (32) and (66) that the effective stiffness matrix $\bar{\mathbf{C}}_P$ for the 2-D cellular material with the periodicity constraints can be obtained as the coefficient matrix of the following constitutive equations:

$$\begin{Bmatrix} \bar{\sigma}_{XX} \\ \bar{\sigma}_{YY} \\ \bar{\sigma}_{XY} \end{Bmatrix} = \begin{bmatrix} \chi_2^P & \chi_3^P & \chi_1^P \\ \chi_3^P & \chi_2^P & \chi_1^P \\ \chi_1^P & \chi_1^P & \chi_4^P \end{bmatrix} \begin{Bmatrix} \bar{\epsilon}_{XX} \\ \bar{\epsilon}_{YY} \\ \bar{\epsilon}_{XY} \end{Bmatrix} = \bar{\mathbf{C}}_P \begin{Bmatrix} \bar{\epsilon}_{XX} \\ \bar{\epsilon}_{YY} \\ \bar{\epsilon}_{XY} \end{Bmatrix},
 \tag{67}$$

where

$$\begin{aligned}
 \chi_1^P &= \frac{k_a}{4} + \frac{k_a^2}{4(k_a+2k_s)}, & \chi_2^P &= \frac{11k_a}{8} - \frac{3k_a^2}{3k_a+k_s} - \frac{k_a^2}{8(k_a+2k_s)}, \\
 \chi_3^P &= -\frac{5k_a}{8} + \frac{3k_a^2}{3k_a+k_s} - \frac{k_a^2}{8(k_a+2k_s)}, & \chi_4^P &= \frac{3k_a}{2} - \frac{k_a^2}{2(k_a+2k_s)}.
 \end{aligned}
 \tag{68}$$

A comparison of Equations (67) and (68) with Equations (55) and (56) shows that the effective stiffness components obtained from the unit cell with the periodicity constraints (see Equation (68)) do not depend on the strut bending stiffness k_b , while those determined from the same unit cell without the periodicity constraints (see Equation (56)) are dependent on k_b as well as k_a and k_s .

3.2. 3-D Cases

3.2.1. Pentamode Metamaterial

Pentamode metamaterials were first proposed by Milton and Cherkaev [48] using a diamond-shaped primitive unit cell shown in Figure 6b. This unit cell can be characterized by three independent primitive lattice vectors (red arrows in Figure 6b). Struts extending from each of the four vertices meet at the center of the cube *C*, which is located inside the primitive cell. This basic structure is repeated periodically in the primitive lattice vector directions to generate the periodic lattice material shown in Figure 6a.

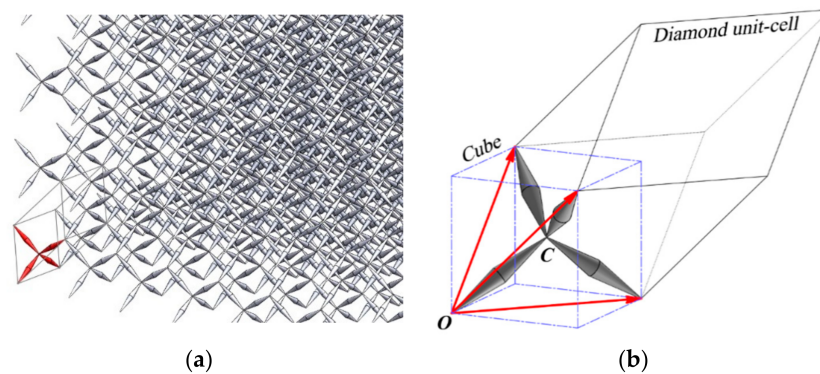


Figure 6. Pentamode metamaterial: (a) microstructure; (b) primitive diamond-shaped unit cell.

The unit cell shown in Figure 6b represents the ideal (perfect) pentamode metamaterial having a zero-shear resistance, where each strut (composed of two truncated cones) overlaps with the other struts at a single point. In the current study, each strut is taken to be a circular cylinder with a uniform cross-section. This allows for a simplified model, while retaining the essential features of the pentamode metamaterial.

The volume and volume fraction of the primitive diamond-shaped unit cell shown in Figure 6b are given by, for struts with a uniform circular cross-section,

$$4V_d = \frac{64L^3}{3\sqrt{3}}, \quad f_d = \frac{3\sqrt{3}\pi}{16} \left(\frac{d}{L}\right)^2, \quad (69)$$

where V_d and f_d are, respectively, the volume and volume fraction of the diamond unit cell, and L and d are, respectively, the length and diameter of each strut. Note that $f_d = V_s/V$ here is the same as the relative density (i.e., $\rho_r \equiv \rho/\rho_s = V_s/V$) (e.g., [20]).

Pentamode metamaterials have been shown to display the isotropic, transversely isotropic or orthotropic symmetry, depending on whether the eigenvalues are distinct or repeated [18]. In addition, pentamode metamaterials can be characterized by three different unit cells: primitive diamond, cubic, and parallelepiped [11]. The parallelepiped unit cell can be obtained from the cubic unit cell through a simple rotation of the coordinate system.

Homogenization in two different coordinate systems shown in Figure 7 is considered in this subsection to understand how the effective engineering constants transform under the coordinate system change.

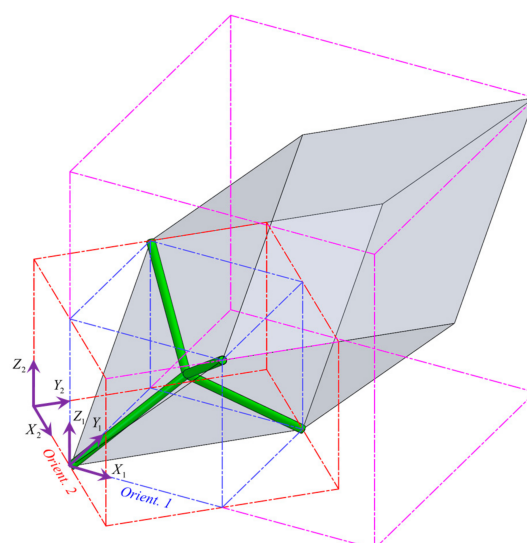


Figure 7. Diamond-shaped unit cell for the pentamode metamaterial in two orientations.

3.2.2. Homogenization without Periodicity Constraints

The generalized strain energy-based homogenization method proposed in Section 2 is applied here to predict the effective elastic properties of the pentamode metamaterial using the diamond-shaped unit cell viewed in two different orientations (coordinate systems) shown in Figure 8a,b. Each of the two representative cells associated with the two orientations in Figure 7 contains four struts of equal lengths L and identical stiffness constants k_a, k_s and k_b , which are the same as those included in the diamond-shaped unit cell shown in Figure 7. In each case, the volume fraction is that of the pentamode metamaterial represented by the primitive diamond-shaped unit cell.

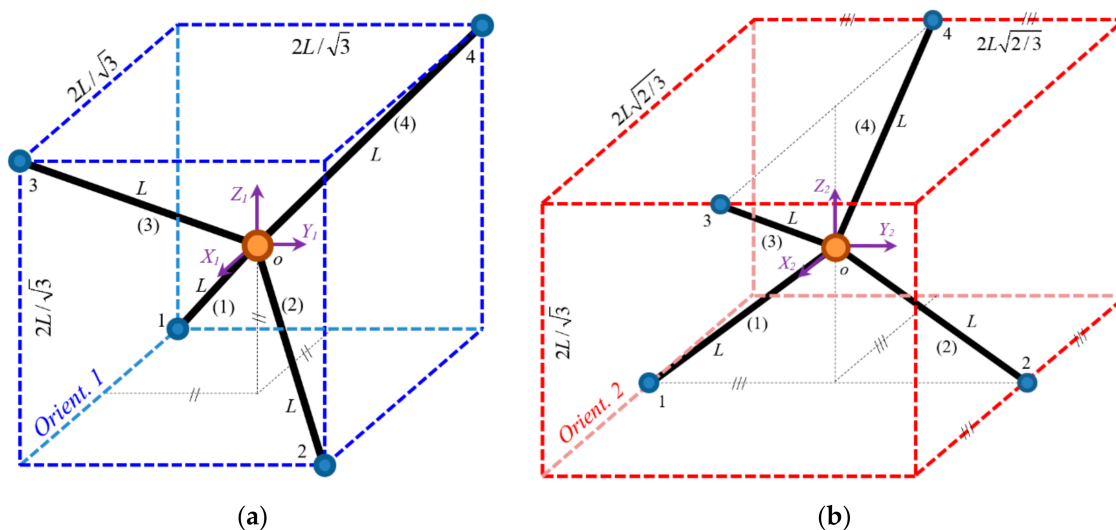


Figure 8. Representative cells for the pentamode metamaterial in two orientations: (a) boundary nodes at four vertices; (b) boundary nodes at mid-points of four edges.

The difference between the two representative cells is that they are 45° apart on the X - Y plane, while the Z -axis is in the same vertical direction in both cases (see Figure 7). That is, the base vectors of the two coordinate systems shown in Figure 8a,b are related through

$$\mathbf{E}_i^{(2)} = \mathbf{Q}\mathbf{E}_i^{(1)}, \quad \mathbf{Q} = \begin{bmatrix} \cos \theta & \sin \theta & 0 \\ -\sin \theta & \cos \theta & 0 \\ 0 & 0 & 1 \end{bmatrix}_{\{\mathbf{E}_i^{(1)} \otimes \mathbf{E}_j^{(1)}\}}, \quad \theta = -45^\circ, \quad i, j \in \{1, 2, 3\}. \quad (70)$$

To construct the pentamode metamaterial from the representative cell in orientation # 1 (the blue cube) in Figures 7 and 8a or Figure 9a, the 4-strut structure in the blue cube is first repeated once along each of the three primitive lattice vector directions (the red arrows in Figure 9a), which results in a new unit cell containing 16 struts enclosed in the pink cube, as displayed in Figure 9b. Then, repeating the 16-strut unit cell in the pink cube along the X_1, Y_1 and Z_1 directions will generate the 3-D periodic pentamode lattice structure, as shown in Figure 9c.

By following a similar procedure, the periodic pentamode lattice metamaterial can be readily constructed from the representative cell in orientation # 2 shown in Figures 7 and 8b.

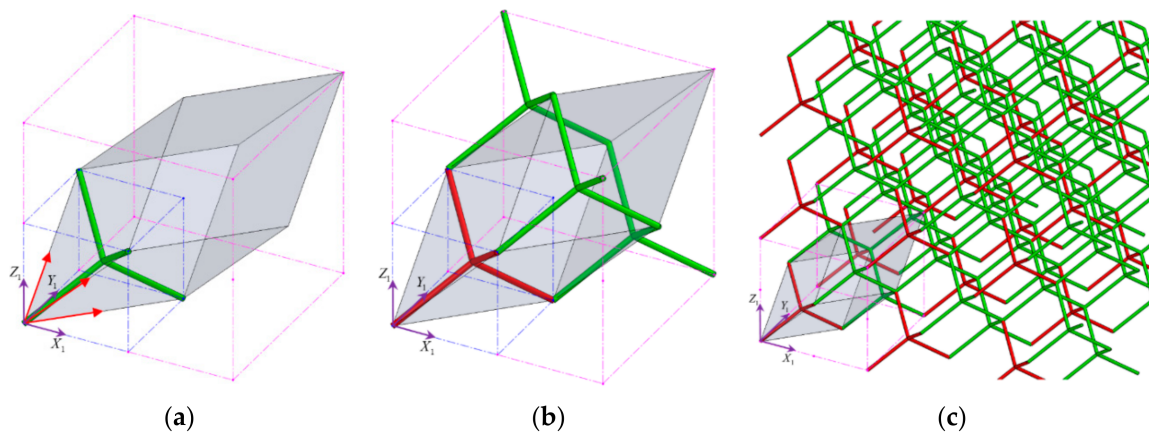


Figure 9. Construction of the pentamode metamaterial from the representative cell in orientation # 1: (a) the representative cell; (b) the new unit cell; (c) the periodic pentamode material.

Homogenization Based on the First Representative Cell

For the representative cell shown in Figure 8a, which will be referred to as orientation # 1, the coordinate transformation matrices for the four struts with respect to the global coordinate system $\{X_1, Y_1, Z_1\}$ can be obtained as

$$\mathbf{Q}^{(1)} = \begin{bmatrix} -\frac{1}{\sqrt{3}} & -\frac{1}{\sqrt{3}} & -\frac{1}{\sqrt{3}} \\ Q_{21}^{(1)} & Q_{22}^{(1)} & Q_{23}^{(1)} \\ Q_{31}^{(1)} & Q_{32}^{(1)} & Q_{33}^{(1)} \end{bmatrix}, \quad \mathbf{Q}^{(2)} = \begin{bmatrix} \frac{1}{\sqrt{3}} & \frac{1}{\sqrt{3}} & -\frac{1}{\sqrt{3}} \\ Q_{21}^{(2)} & Q_{22}^{(2)} & Q_{23}^{(2)} \\ Q_{31}^{(2)} & Q_{32}^{(2)} & Q_{33}^{(2)} \end{bmatrix}, \quad (71)$$

$$\mathbf{Q}^{(3)} = \begin{bmatrix} \frac{1}{\sqrt{3}} & -\frac{1}{\sqrt{3}} & \frac{1}{\sqrt{3}} \\ Q_{21}^{(3)} & Q_{22}^{(3)} & Q_{23}^{(3)} \\ Q_{31}^{(3)} & Q_{32}^{(3)} & Q_{33}^{(3)} \end{bmatrix}, \quad \mathbf{Q}^{(4)} = \begin{bmatrix} -\frac{1}{\sqrt{3}} & \frac{1}{\sqrt{3}} & \frac{1}{\sqrt{3}} \\ Q_{21}^{(4)} & Q_{22}^{(4)} & Q_{23}^{(4)} \\ Q_{31}^{(4)} & Q_{32}^{(4)} & Q_{33}^{(4)} \end{bmatrix},$$

where the unspecified components of each $\mathbf{Q}^{(k)}$ matrix can be arbitrarily chosen as long as the matrix is proper orthogonal with

$$[\mathbf{Q}^{(k)}]^{-1} = [\mathbf{Q}^{(k)}]^T, \quad \det(\mathbf{Q}^{(k)}) = 1. \quad (72)$$

This is due to the fact that the cross-section of each strut is circular, so that the local coordinate axes y and z can be arbitrarily oriented on a cross-section. Based on these constraints, the following transformation matrices with respect to the coordinate system $\{X_1, Y_1, Z_1\}$ have been chosen:

$$\mathbf{Q}^{(1)} = \begin{bmatrix} -\frac{1}{\sqrt{3}} & -\frac{1}{\sqrt{3}} & -\frac{1}{\sqrt{3}} \\ \frac{1}{\sqrt{6}} & -\sqrt{\frac{2}{3}} & \frac{1}{\sqrt{6}} \\ -\frac{1}{\sqrt{2}} & 0 & \frac{1}{\sqrt{2}} \end{bmatrix}, \quad \mathbf{Q}^{(2)} = \begin{bmatrix} \frac{1}{\sqrt{3}} & \frac{1}{\sqrt{3}} & -\frac{1}{\sqrt{3}} \\ \frac{1}{\sqrt{6}} & \frac{1}{\sqrt{6}} & \sqrt{\frac{2}{3}} \\ \frac{1}{\sqrt{2}} & -\frac{1}{\sqrt{2}} & 0 \end{bmatrix}, \quad (73)$$

$$\mathbf{Q}^{(3)} = \begin{bmatrix} \frac{1}{\sqrt{3}} & -\frac{1}{\sqrt{3}} & \frac{1}{\sqrt{3}} \\ \frac{1}{\sqrt{6}} & \sqrt{\frac{2}{3}} & \frac{1}{\sqrt{6}} \\ -\frac{1}{\sqrt{2}} & 0 & \frac{1}{\sqrt{2}} \end{bmatrix}, \quad \mathbf{Q}^{(4)} = \begin{bmatrix} -\frac{1}{\sqrt{3}} & \frac{1}{\sqrt{3}} & \frac{1}{\sqrt{3}} \\ \sqrt{\frac{2}{3}} & \frac{1}{\sqrt{6}} & \frac{1}{\sqrt{6}} \\ 0 & \frac{1}{\sqrt{2}} & -\frac{1}{\sqrt{2}} \end{bmatrix}.$$

In addition, the position vector for each of the five nodes in the unit cell shown in Figure 8a can be written in terms of the global coordinates $\{X_1, Y_1, Z_1\}$ as

$$\begin{aligned} \mathbf{X}_1 &= -\frac{L}{\sqrt{3}} \{ 1 \ 1 \ 1 \}^T, \quad \mathbf{X}_2 = \frac{L}{\sqrt{3}} \{ 1 \ 1 \ -1 \}^T, \\ \mathbf{X}_3 &= \frac{L}{\sqrt{3}} \{ 1 \ -1 \ 1 \}^T, \quad \mathbf{X}_4 = \frac{L}{\sqrt{3}} \{ -1 \ 1 \ 1 \}^T, \quad \mathbf{X}_5 = \{ 0 \ 0 \ 0 \}^T. \end{aligned} \quad (74)$$

According to the generalized strain energy-based homogenization method formulated in Section 2.3, this representative cell can be characterized by $P = 4$, $Q = 0$, $M = 1$ and $N = 4$. Substituting Equations (18) and (74) into Equation (22) gives the boundary conditions at the four boundary nodes as

$$\begin{aligned} \begin{Bmatrix} u_{X_11} \\ u_{Y_11} \\ u_{Z_11} \end{Bmatrix} &= -\frac{L}{\sqrt{3}} \begin{Bmatrix} \bar{\varepsilon}_{X_1X_1} + \bar{\varepsilon}_{X_1Y_1} + \bar{\varepsilon}_{X_1Z_1} \\ \bar{\varepsilon}_{X_1Y_1} + \bar{\varepsilon}_{Y_1Y_1} + \bar{\varepsilon}_{Y_1Z_1} \\ \bar{\varepsilon}_{X_1Z_1} + \bar{\varepsilon}_{Y_1Z_1} + \bar{\varepsilon}_{Z_1Z_1} \end{Bmatrix}, \quad \begin{Bmatrix} u_{X_12} \\ u_{Y_12} \\ u_{Z_12} \end{Bmatrix} = \frac{L}{\sqrt{3}} \begin{Bmatrix} \bar{\varepsilon}_{X_1X_1} + \bar{\varepsilon}_{X_1Y_1} - \bar{\varepsilon}_{X_1Z_1} \\ \bar{\varepsilon}_{X_1Y_1} + \bar{\varepsilon}_{Y_1Y_1} - \bar{\varepsilon}_{Y_1Z_1} \\ \bar{\varepsilon}_{X_1Z_1} + \bar{\varepsilon}_{Y_1Z_1} - \bar{\varepsilon}_{Z_1Z_1} \end{Bmatrix}, \\ \begin{Bmatrix} u_{X_13} \\ u_{Y_13} \\ u_{Z_13} \end{Bmatrix} &= \frac{L}{\sqrt{3}} \begin{Bmatrix} \bar{\varepsilon}_{X_1X_1} - \bar{\varepsilon}_{X_1Y_1} + \bar{\varepsilon}_{X_1Z_1} \\ \bar{\varepsilon}_{X_1Y_1} - \bar{\varepsilon}_{Y_1Y_1} + \bar{\varepsilon}_{Y_1Z_1} \\ \bar{\varepsilon}_{X_1Z_1} - \bar{\varepsilon}_{Y_1Z_1} + \bar{\varepsilon}_{Z_1Z_1} \end{Bmatrix}, \quad \begin{Bmatrix} u_{X_14} \\ u_{Y_14} \\ u_{Z_14} \end{Bmatrix} = \frac{L}{\sqrt{3}} \begin{Bmatrix} -\bar{\varepsilon}_{X_1X_1} + \bar{\varepsilon}_{X_1Y_1} + \bar{\varepsilon}_{X_1Z_1} \\ -\bar{\varepsilon}_{X_1Y_1} + \bar{\varepsilon}_{Y_1Y_1} + \bar{\varepsilon}_{Y_1Z_1} \\ -\bar{\varepsilon}_{X_1Z_1} + \bar{\varepsilon}_{Y_1Z_1} + \bar{\varepsilon}_{Z_1Z_1} \end{Bmatrix}, \\ \begin{Bmatrix} M_{X_11} \\ M_{Y_11} \\ M_{Z_11} \end{Bmatrix} &= \begin{Bmatrix} M_{X_12} \\ M_{Y_12} \\ M_{Z_12} \end{Bmatrix} = \begin{Bmatrix} M_{X_13} \\ M_{Y_13} \\ M_{Z_13} \end{Bmatrix} = \begin{Bmatrix} M_{X_14} \\ M_{Y_14} \\ M_{Z_14} \end{Bmatrix} = \begin{Bmatrix} 0 \\ 0 \\ 0 \end{Bmatrix}. \end{aligned} \quad (75)$$

Using Equations (1), (2), (7), (9), (12), (13), (73) and (75) in Equation (30) or Equation (76) leads to the rotation components at the four boundary nodes as

$$\begin{Bmatrix} \theta_{X_11} \\ \theta_{Y_11} \\ \theta_{Z_11} \end{Bmatrix} = \begin{Bmatrix} \theta_{X_1o} + \frac{Lk_s(-L\bar{\varepsilon}_{X_1Y_1} + L\bar{\varepsilon}_{X_1Z_1} - L\bar{\varepsilon}_{Y_1Y_1} + L\bar{\varepsilon}_{Z_1Z_1} - 2L\theta_{X_1o} + L\theta_{Y_1o} + L\theta_{Z_1o} - \sqrt{3}u_{Y_1o} + \sqrt{3}u_{Z_1o})}{6k_b} \\ \theta_{Y_1o} + \frac{Lk_s(L\bar{\varepsilon}_{X_1X_1} + L\bar{\varepsilon}_{X_1Y_1} - L\bar{\varepsilon}_{Y_1Z_1} - L\bar{\varepsilon}_{Z_1Z_1} + L\theta_{X_1o} - 2L\theta_{Y_1o} + L\theta_{Z_1o} + \sqrt{3}u_{X_1o} - \sqrt{3}u_{Z_1o})}{6k_b} \\ \theta_{Z_1o} + \frac{Lk_s(-L\bar{\varepsilon}_{X_1X_1} - L\bar{\varepsilon}_{X_1Z_1} + L\bar{\varepsilon}_{Y_1Y_1} + L\bar{\varepsilon}_{Y_1Z_1} + L\theta_{X_1o} + L\theta_{Y_1o} - 2L\theta_{Z_1o} - \sqrt{3}u_{X_1o} + \sqrt{3}u_{Y_1o})}{6k_b} \end{Bmatrix}, \quad (77)$$

$$\begin{Bmatrix} \theta_{X_12} \\ \theta_{Y_12} \\ \theta_{Z_12} \end{Bmatrix} = \begin{Bmatrix} \theta_{X_1o} - \frac{Lk_s(-L\bar{\varepsilon}_{X_1Y_1} - L\bar{\varepsilon}_{X_1Z_1} - L\bar{\varepsilon}_{Y_1Y_1} + L\bar{\varepsilon}_{Z_1Z_1} + 2L\theta_{X_1o} - L\theta_{Y_1o} + L\theta_{Z_1o} + \sqrt{3}u_{Y_1o} + \sqrt{3}u_{Z_1o})}{6k_b} \\ \theta_{Y_1o} - \frac{Lk_s(L\bar{\varepsilon}_{X_1X_1} + L\bar{\varepsilon}_{X_1Y_1} + L\bar{\varepsilon}_{Y_1Z_1} - L\bar{\varepsilon}_{Z_1Z_1} - L\theta_{X_1o} + 2L\theta_{Y_1o} + L\theta_{Z_1o} - \sqrt{3}u_{X_1o} - \sqrt{3}u_{Z_1o})}{6k_b} \\ \theta_{Z_1o} - \frac{Lk_s(L\bar{\varepsilon}_{X_1X_1} - L\bar{\varepsilon}_{X_1Z_1} - L\bar{\varepsilon}_{Y_1Y_1} + L\bar{\varepsilon}_{Y_1Z_1} + L\theta_{X_1o} + L\theta_{Y_1o} + 2L\theta_{Z_1o} - \sqrt{3}u_{X_1o} + \sqrt{3}u_{Y_1o})}{6k_b} \end{Bmatrix}, \quad (78)$$

$$\begin{Bmatrix} \theta_{X_13} \\ \theta_{Y_13} \\ \theta_{Z_13} \end{Bmatrix} = \begin{Bmatrix} \theta_{X_1o} - \frac{Lk_s(L\bar{\varepsilon}_{X_1Y_1} + L\bar{\varepsilon}_{X_1Z_1} - L\bar{\varepsilon}_{Y_1Y_1} + L\bar{\varepsilon}_{Z_1Z_1} + 2L\theta_{X_1o} + L\theta_{Y_1o} - L\theta_{Z_1o} - \sqrt{3}u_{Y_1o} - \sqrt{3}u_{Z_1o})}{6k_b} \\ \theta_{Y_1o} - \frac{Lk_s(-L\bar{\varepsilon}_{X_1X_1} + L\bar{\varepsilon}_{X_1Y_1} - L\bar{\varepsilon}_{Y_1Z_1} + L\bar{\varepsilon}_{Z_1Z_1} + L\theta_{X_1o} + 2L\theta_{Y_1o} + L\theta_{Z_1o} + \sqrt{3}u_{X_1o} - \sqrt{3}u_{Z_1o})}{6k_b} \\ \theta_{Z_1o} - \frac{Lk_s(-L\bar{\varepsilon}_{X_1X_1} - L\bar{\varepsilon}_{X_1Z_1} + L\bar{\varepsilon}_{Y_1Y_1} - L\bar{\varepsilon}_{Y_1Z_1} - L\theta_{X_1o} + L\theta_{Y_1o} + 2L\theta_{Z_1o} + \sqrt{3}u_{X_1o} + \sqrt{3}u_{Y_1o})}{6k_b} \end{Bmatrix}, \quad (79)$$

$$\begin{Bmatrix} \theta_{X_14} \\ \theta_{Y_14} \\ \theta_{Z_14} \end{Bmatrix} = \begin{Bmatrix} \theta_{X_1o} - \frac{Lk_s(-L\bar{\varepsilon}_{X_1Y_1} + L\bar{\varepsilon}_{X_1Z_1} + L\bar{\varepsilon}_{Y_1Y_1} - L\bar{\varepsilon}_{Z_1Z_1} + 2L\theta_{X_1o} + L\theta_{Y_1o} + L\theta_{Z_1o} - \sqrt{3}u_{Y_1o} + \sqrt{3}u_{Z_1o})}{6k_b} \\ \theta_{Y_1o} - \frac{Lk_s(L\bar{\varepsilon}_{X_1X_1} - L\bar{\varepsilon}_{X_1Y_1} - L\bar{\varepsilon}_{Y_1Z_1} - L\bar{\varepsilon}_{Z_1Z_1} + L\theta_{X_1o} + 2L\theta_{Y_1o} - L\theta_{Z_1o} + \sqrt{3}u_{X_1o} + \sqrt{3}u_{Z_1o})}{6k_b} \\ \theta_{Z_1o} - \frac{Lk_s(-L\bar{\varepsilon}_{X_1X_1} + L\bar{\varepsilon}_{X_1Z_1} + L\bar{\varepsilon}_{Y_1Y_1} + L\bar{\varepsilon}_{Y_1Z_1} + L\theta_{X_1o} - L\theta_{Y_1o} + 2L\theta_{Z_1o} - \sqrt{3}u_{X_1o} - \sqrt{3}u_{Y_1o})}{6k_b} \end{Bmatrix}. \quad (80)$$

Substituting Equations (1), (2), (7), (9), (12), (13), (73) and (77)–(80) into the equilibrium equations at the interior node in Equation (31) yields the displacement and rotation components at the central node o as

$$\begin{Bmatrix} u_{X_1o} \\ u_{Y_1o} \\ u_{Z_1o} \\ \theta_{X_1o} \\ \theta_{Y_1o} \\ \theta_{Z_1o} \end{Bmatrix} = \begin{Bmatrix} \left(\frac{\sqrt{3}L}{3} - \frac{2\sqrt{3}Lk_a k_b}{2k_a k_b + 4k_b k_s - L^2 k_s^2} \right) \bar{\epsilon}_{Y_1 Z_1} \\ \left(\frac{\sqrt{3}L}{3} - \frac{2\sqrt{3}Lk_a k_b}{2k_a k_b + 4k_b k_s - L^2 k_s^2} \right) \bar{\epsilon}_{X_1 Z_1} \\ \left(\frac{\sqrt{3}L}{3} - \frac{2\sqrt{3}Lk_a k_b}{2k_a k_b + 4k_b k_s - L^2 k_s^2} \right) \bar{\epsilon}_{X_1 Y_1} \\ 0 \\ 0 \\ 0 \end{Bmatrix}. \quad (81)$$

It follows from Equations (1), (2), (7), (9), (15), (25), (29), (73), (75), (77)–(80) and (81) that the strain energy density function in this case has the form:

$$\begin{aligned} u = & \frac{\sqrt{3}}{24} \left(\frac{k_a + 2k_s}{L} - \frac{Lk_s^2}{2k_b} \right) \left(\bar{\epsilon}_{X_1 X_1}^2 + \bar{\epsilon}_{Y_1 Y_1}^2 + \bar{\epsilon}_{Z_1 Z_1}^2 \right) \\ & + \frac{3\sqrt{3}k_a k_s}{8(k_a + 2k_s)} \left(\frac{2}{L} - \frac{Lk_a k_s}{2k_a k_b + 4k_b k_s - L^2 k_s^2} \right) \left(\bar{\epsilon}_{X_1 Y_1}^2 + \bar{\epsilon}_{X_1 Z_1}^2 + \bar{\epsilon}_{Y_1 Z_1}^2 \right) \\ & + \frac{\sqrt{3}}{12} \left(\frac{k_a - k_s}{L} + \frac{Lk_s^2}{4k_b} \right) \left(\bar{\epsilon}_{X_1 X_1} \bar{\epsilon}_{Y_1 Y_1} + \bar{\epsilon}_{X_1 X_1} \bar{\epsilon}_{Z_1 Z_1} + \bar{\epsilon}_{Y_1 Y_1} \bar{\epsilon}_{Z_1 Z_1} \right), \end{aligned} \quad (82)$$

which does not involve any unknown kinematic variable.

Finally, from Equations (32) and (82) the effective stiffness matrix $\bar{\mathbf{C}}^{(1)}$ for the pentamode metamaterial based on the representative cell in orientation # 1 shown in Figure 8a can be obtained as the coefficient matrix of the following constitutive equations:

$$\begin{Bmatrix} \bar{\sigma}_{X_1 X_1} \\ \bar{\sigma}_{Y_1 Y_1} \\ \bar{\sigma}_{Z_1 Z_1} \\ \bar{\sigma}_{Y_1 Z_1} \\ \bar{\sigma}_{X_1 Z_1} \\ \bar{\sigma}_{X_1 Y_1} \end{Bmatrix} = \begin{bmatrix} \chi_{1M}^{(1)} & \chi_{2M}^{(1)} & \chi_{2M}^{(1)} & 0 & 0 & 0 \\ \chi_{2M}^{(1)} & \chi_{1M}^{(1)} & \chi_{2M}^{(1)} & 0 & 0 & 0 \\ \chi_{2M}^{(1)} & \chi_{2M}^{(1)} & \chi_{1M}^{(1)} & 0 & 0 & 0 \\ 0 & 0 & 0 & \chi_{3M}^{(1)} & 0 & 0 \\ 0 & 0 & 0 & 0 & \chi_{3M}^{(1)} & 0 \\ 0 & 0 & 0 & 0 & 0 & \chi_{3M}^{(1)} \end{bmatrix} \begin{Bmatrix} \bar{\epsilon}_{X_1 X_1} \\ \bar{\epsilon}_{Y_1 Y_1} \\ \bar{\epsilon}_{Z_1 Z_1} \\ \bar{\epsilon}_{Y_1 Z_1} \\ \bar{\epsilon}_{X_1 Z_1} \\ \bar{\epsilon}_{X_1 Y_1} \end{Bmatrix} = \bar{\mathbf{C}}^{(1)} \begin{Bmatrix} \bar{\epsilon}_{X_1 X_1} \\ \bar{\epsilon}_{Y_1 Y_1} \\ \bar{\epsilon}_{Z_1 Z_1} \\ \bar{\epsilon}_{Y_1 Z_1} \\ \bar{\epsilon}_{X_1 Z_1} \\ \bar{\epsilon}_{X_1 Y_1} \end{Bmatrix}, \quad (83)$$

where

$$\begin{aligned} \chi_{1M}^{(1)} &= \frac{\sqrt{3}(k_a + 2k_s)}{12L} - \frac{\sqrt{3}Lk_s^2}{24k_b}, & \chi_{2M}^{(1)} &= \frac{\sqrt{3}(k_a - k_s)}{12L} + \frac{\sqrt{3}Lk_s^2}{48k_b}, \\ \chi_{3M}^{(1)} &= \frac{3\sqrt{3}k_a k_s (4k_b - L^2 k_s)}{4L(2k_a k_b + 4k_b k_s - L^2 k_s^2)}. \end{aligned} \quad (84)$$

It is clear that the stiffness matrix $\bar{\mathbf{C}}^{(1)}$ depends on only three constants $\chi_{1M}^{(1)}$, $\chi_{2M}^{(1)}$ and $\chi_{3M}^{(1)}$, which indicates that the pentamode metamaterial possesses the cubic symmetry in the current case with the representative cell in orientation # 1. These stiffness constants are the same as those obtained in [18] for the pentamode material with the diamond unit cell using an equilibrium equation-based approach, thereby providing a validation of the current model.

The effective compliance matrix $\bar{\mathbf{S}}^{(1)} = [\bar{\mathbf{C}}^{(1)}]^{-1}$ based on the representative cell in orientation # 1 can be readily obtained from Equations (83) and (84) as

$$\bar{\mathbf{S}}^{(1)} = \begin{bmatrix} \zeta_{1M}^{(1)} & \zeta_{2M}^{(1)} & \zeta_{2M}^{(1)} & 0 & 0 & 0 \\ \zeta_{2M}^{(1)} & \zeta_{1M}^{(1)} & \zeta_{2M}^{(1)} & 0 & 0 & 0 \\ \zeta_{2M}^{(1)} & \zeta_{2M}^{(1)} & \zeta_{1M}^{(1)} & 0 & 0 & 0 \\ 0 & 0 & 0 & \zeta_{3M}^{(1)} & 0 & 0 \\ 0 & 0 & 0 & 0 & \zeta_{3M}^{(1)} & 0 \\ 0 & 0 & 0 & 0 & 0 & \zeta_{3M}^{(1)} \end{bmatrix}, \quad (85)$$

where

$$\begin{aligned} \zeta_{1M}^{(1)} &= \frac{4\sqrt{3}L}{9k_a} + \frac{32\sqrt{3}Lk_b}{9k_s(4k_b - L^2k_s)}, & \zeta_{2M}^{(1)} &= \frac{4\sqrt{3}L}{9k_a} - \frac{16\sqrt{3}Lk_b}{9k_s(4k_b - L^2k_s)}, \\ \zeta_{3M}^{(1)} &= \frac{4\sqrt{3}L}{9k_a} + \frac{8\sqrt{3}Lk_b}{9k_s(4k_b - L^2k_s)}. \end{aligned} \quad (86)$$

For a cubic material, the directional dependence of the engineering constants can be described by (e.g., [49,50])

$$\begin{aligned} \bar{E}(\mathbf{n}) &= \frac{1}{\bar{S}_{11}} = \left[\frac{1}{9\kappa} + \frac{1}{3\mu_2} - \left(\frac{1}{\mu_2} - \frac{1}{\mu_1} \right) F(\mathbf{n}) \right]^{-1}, \\ \bar{G}(\mathbf{n}, \mathbf{m}) &= \frac{1}{4\bar{S}_{66}} = \left[\frac{1}{\mu_1} + 2 \left(\frac{1}{\mu_2} - \frac{1}{\mu_1} \right) D(\mathbf{n}, \mathbf{m}) \right]^{-1}, \\ \bar{\nu}(\mathbf{n}, \mathbf{m}) &= -\frac{\bar{S}_{12}}{\bar{S}_{11}} = \bar{E}(\mathbf{n}) \left[-\frac{1}{9\kappa} + \frac{1}{6\mu_2} - \frac{1}{2} \left(\frac{1}{\mu_2} - \frac{1}{\mu_1} \right) D(\mathbf{n}, \mathbf{m}) \right], \end{aligned} \quad (87)$$

where \bar{E} , \bar{G} and $\bar{\nu}$ are, respectively, the effective Young's modulus, shear modulus and Poisson's ratio, κ , μ_1 and μ_2 are the three principal elastic constants given by

$$\kappa = \frac{\bar{C}_{11} + 2\bar{C}_{12}}{3}, \quad \mu_1 = \frac{\bar{C}_{66}}{4}, \quad \mu_2 = \frac{\bar{C}_{11} - \bar{C}_{12}}{2}, \quad (88)$$

$\{\mathbf{n}, \mathbf{m}, \mathbf{t}\}$ is an orthonormal set of unit vectors, and $F(\mathbf{n})$ and $D(\mathbf{n}, \mathbf{m})$ are defined as

$$F(\mathbf{n}) = n_1^2 n_2^2 + n_2^2 n_3^2 + n_3^2 n_1^2, \quad D(\mathbf{n}, \mathbf{m}) = n_1^2 m_1^2 + n_2^2 m_2^2 + n_3^2 m_3^2, \quad (89)$$

with $\mathbf{n} = (n_1, n_2, n_3)$ and $\mathbf{m} = (m_1, m_2, m_3)$.

Consider the triad $\{\mathbf{n}^o, \mathbf{m}^o, \mathbf{t}^o\}$ aligned with the base vectors $\{\mathbf{E}_1^{(1)}, \mathbf{E}_2^{(1)}, \mathbf{E}_3^{(1)}\}$ of the coordinate system in Figure 8a with $\mathbf{n}^o = \mathbf{E}_1^{(1)}$, $\mathbf{m}^o = \mathbf{E}_2^{(1)}$, $\mathbf{t}^o = \mathbf{E}_3^{(1)}$, and the triad $\{\mathbf{n}^f, \mathbf{m}^f, \mathbf{t}^f\}$ aligned with the base vectors $\{\mathbf{E}_1^{(2)}, \mathbf{E}_2^{(2)}, \mathbf{E}_3^{(2)}\}$ of the coordinate system in Figure 8b with $\mathbf{n}^f = \mathbf{E}_1^{(2)}$, $\mathbf{m}^f = \mathbf{E}_2^{(2)}$, $\mathbf{t}^f = \mathbf{E}_3^{(2)}$. Since $\mathbf{E}_3^{(1)}$ remains unchanged (with $\mathbf{E}_3^{(1)} = \mathbf{E}_3^{(2)}$), \mathbf{n} and \mathbf{m} , which are two orthonormal vectors rotated from $\mathbf{E}_1^{(1)}$ and $\mathbf{E}_2^{(1)}$ by an angle of θ , can be obtained as

$$\mathbf{n} = \mathbf{E}_1^{(1)} \cos \theta + \mathbf{E}_2^{(1)} \sin \theta, \quad \mathbf{m} = -\mathbf{E}_1^{(1)} \sin \theta + \mathbf{E}_2^{(1)} \cos \theta. \quad (90)$$

Using Equations (83), (84) and (88)–(90) in Equation (87) leads to

$$\begin{aligned} \bar{E}_{hom}(\theta) &= \frac{3\sqrt{3}k_a k_s (4k_b - L^2 k_s)}{2L [3(4k_a k_b + 4k_b k_s - L^2 k_s^2) + (4k_a k_b - 4k_b k_s + L^2 k_s^2) \cos(4\theta)]}, \\ \bar{G}_{hom}(\theta) &= \frac{3\sqrt{3}k_a k_s (4k_b - L^2 k_s)}{16L [6k_a k_b + (-4k_a k_b + 4k_b k_s - L^2 k_s^2) \cos^2(2\theta)]}, \\ \bar{\nu}_{hom}(\theta) &= \frac{(4k_a k_b - 4k_b k_s + L^2 k_s^2) [1 + \cos(4\theta)]}{3(4k_a k_b + 4k_b k_s - L^2 k_s^2) + (4k_a k_b - 4k_b k_s + L^2 k_s^2) \cos(4\theta)}. \end{aligned} \quad (91)$$

which establish the functional relations between the effective engineering constants and the angle θ for the pentamode metamaterial using the stiffness matrix based on the representative cell in orientation # 1 shown in Figure 8a.

Homogenization Based on the Second Representative Cell

For the representative cell in orientation # 2 shown in Figure 8b, the coordinate transformation matrix with respect to the coordinate system $\{X_2, Y_2, Z_2\}$ for each strut satisfying Equation (72) is selected to be

$$\mathbf{Q}^{(1)} = \begin{bmatrix} 0 & -\sqrt{\frac{2}{3}} & -\frac{1}{\sqrt{3}} \\ 0 & -\frac{1}{\sqrt{3}} & \sqrt{\frac{2}{3}} \\ -1 & 0 & 0 \end{bmatrix}, \quad \mathbf{Q}^{(2)} = \begin{bmatrix} 0 & \sqrt{\frac{2}{3}} & -\frac{1}{\sqrt{3}} \\ 0 & -\frac{1}{\sqrt{3}} & -\sqrt{\frac{2}{3}} \\ -1 & 0 & 0 \end{bmatrix}, \quad (92)$$

$$\mathbf{Q}^{(3)} = \begin{bmatrix} \sqrt{\frac{2}{3}} & 0 & \frac{1}{\sqrt{3}} \\ \frac{1}{\sqrt{3}} & 0 & -\sqrt{\frac{2}{3}} \\ 0 & 1 & 0 \end{bmatrix}, \quad \mathbf{Q}^{(4)} = \begin{bmatrix} -\sqrt{\frac{2}{3}} & 0 & \frac{1}{\sqrt{3}} \\ \frac{1}{\sqrt{3}} & 0 & \sqrt{\frac{2}{3}} \\ 0 & 1 & 0 \end{bmatrix}.$$

In addition, the position vector for each of the five nodes in the representative cell in Figure 8b with respect to the coordinate system $\{X_2, Y_2, Z_2\}$ can be written as

$$\mathbf{x}_1 = L \left\{ 0 \quad -\sqrt{\frac{2}{3}} \quad -\frac{1}{\sqrt{3}} \right\}^T, \quad \mathbf{x}_2 = L \left\{ 0 \quad \sqrt{\frac{2}{3}} \quad -\frac{1}{\sqrt{3}} \right\}^T, \quad (93)$$

$$\mathbf{x}_3 = L \left\{ \sqrt{\frac{2}{3}} \quad 0 \quad \frac{1}{\sqrt{3}} \right\}^T, \quad \mathbf{x}_4 = L \left\{ -\sqrt{\frac{2}{3}} \quad 0 \quad \frac{1}{\sqrt{3}} \right\}^T, \quad \mathbf{x}_5 = \{ 0 \quad 0 \quad 0 \}^T.$$

Substituting Equations (18) and (93) into Equation (22) gives the boundary conditions at the four boundary nodes as

$$\begin{cases} u_{X_21} \\ u_{Y_21} \\ u_{Z_21} \end{cases} = -\frac{L}{\sqrt{3}} \begin{cases} \sqrt{2}\bar{\epsilon}_{X_2Y_2} + \bar{\epsilon}_{X_2Z_2} \\ \sqrt{2}\bar{\epsilon}_{Y_2Y_2} + \bar{\epsilon}_{Y_2Z_2} \\ \sqrt{2}\bar{\epsilon}_{Y_2Z_2} + \bar{\epsilon}_{Z_2Z_2} \end{cases}, \quad \begin{cases} u_{X_22} \\ u_{Y_22} \\ u_{Z_22} \end{cases} = \frac{L}{\sqrt{3}} \begin{cases} \sqrt{2}\bar{\epsilon}_{X_2Y_2} - \bar{\epsilon}_{X_2Z_2} \\ \sqrt{2}\bar{\epsilon}_{Y_2Y_2} - \bar{\epsilon}_{Y_2Z_2} \\ \sqrt{2}\bar{\epsilon}_{Y_2Z_2} - \bar{\epsilon}_{Z_2Z_2} \end{cases}, \quad (94)$$

$$\begin{cases} u_{X_23} \\ u_{Y_23} \\ u_{Z_23} \end{cases} = \frac{L}{\sqrt{3}} \begin{cases} \sqrt{2}\bar{\epsilon}_{X_2X_2} + \bar{\epsilon}_{X_2Z_2} \\ \sqrt{2}\bar{\epsilon}_{X_2Y_2} + \bar{\epsilon}_{Y_2Z_2} \\ \sqrt{2}\bar{\epsilon}_{X_2Z_2} + \bar{\epsilon}_{Z_2Z_2} \end{cases}, \quad \begin{cases} u_{X_24} \\ u_{Y_24} \\ u_{Z_24} \end{cases} = \frac{L}{\sqrt{3}} \begin{cases} -\sqrt{2}\bar{\epsilon}_{X_2X_2} + \bar{\epsilon}_{X_2Z_2} \\ -\sqrt{2}\bar{\epsilon}_{X_2Y_2} + \bar{\epsilon}_{Y_2Z_2} \\ -\sqrt{2}\bar{\epsilon}_{X_2Z_2} + \bar{\epsilon}_{Z_2Z_2} \end{cases},$$

$$\begin{cases} M_{X_21} \\ M_{Y_21} \\ M_{Z_21} \end{cases} = \begin{cases} M_{X_22} \\ M_{Y_22} \\ M_{Z_22} \end{cases} = \begin{cases} M_{X_23} \\ M_{Y_23} \\ M_{Z_23} \end{cases} = \begin{cases} M_{X_24} \\ M_{Y_24} \\ M_{Z_24} \end{cases} = \begin{cases} 0 \\ 0 \\ 0 \end{cases}. \quad (95)$$

Using Equations (1), (2), (7), (9), (12), (13), (92) and (94) in Equation (30) or Equation (95) yields the rotation components at the four boundary nodes as

$$\begin{cases} \theta_{X_21} \\ \theta_{Y_21} \\ \theta_{Z_21} \end{cases} = \begin{cases} \theta_{X_20} + \frac{Lk_s(-\sqrt{2}L\bar{\epsilon}_{Y_2Y_2} + L\bar{\epsilon}_{Y_2Z_2} + \sqrt{2}L\bar{\epsilon}_{Z_2Z_2} - \sqrt{3}u_{Y_20} + \sqrt{6}u_{Z_20} - 3L\theta_{X_20})}{6k_b} \\ \theta_{Y_20} + \frac{Lk_s(\sqrt{2}L\bar{\epsilon}_{X_2Y_2} + L\bar{\epsilon}_{X_2Z_2} + \sqrt{3}u_{X_20} - L\theta_{Y_20} + \sqrt{2}L\theta_{Z_20})}{6k_b} \\ \theta_{Z_20} - \frac{Lk_s(2L\bar{\epsilon}_{X_2Y_2} + \sqrt{2}L\bar{\epsilon}_{X_2Z_2} + \sqrt{6}u_{X_20} - \sqrt{2}L\theta_{Y_20} + 2L\theta_{Z_20})}{6k_b} \end{cases}, \quad (96)$$

$$\begin{cases} \theta_{X_22} \\ \theta_{Y_22} \\ \theta_{Z_22} \end{cases} = \begin{cases} \theta_{X_20} - \frac{Lk_s(-\sqrt{2}L\bar{\epsilon}_{Y_2Y_2} - L\bar{\epsilon}_{Y_2Z_2} + \sqrt{2}L\bar{\epsilon}_{Z_2Z_2} + \sqrt{3}u_{Y_20} + \sqrt{6}u_{Z_20} + 3L\theta_{X_20})}{6k_b} \\ \theta_{Y_20} - \frac{Lk_s(\sqrt{2}L\bar{\epsilon}_{X_2Y_2} - L\bar{\epsilon}_{X_2Z_2} - \sqrt{3}u_{X_20} + L\theta_{Y_20} + \sqrt{2}L\theta_{Z_20})}{6k_b} \\ \theta_{Z_20} - \frac{Lk_s(2L\bar{\epsilon}_{X_2Y_2} - \sqrt{2}L\bar{\epsilon}_{X_2Z_2} - \sqrt{6}u_{X_20} + \sqrt{2}L\theta_{Y_20} + 2L\theta_{Z_20})}{6k_b} \end{cases}, \quad (97)$$

$$\begin{Bmatrix} \theta_{X_2 3} \\ \theta_{Y_2 3} \\ \theta_{Z_2 3} \end{Bmatrix} = \begin{Bmatrix} \theta_{X_2 0} - \frac{Lk_s(\sqrt{2L}\bar{\epsilon}_{X_2 Y_2} + L\bar{\epsilon}_{Y_2 Z_2} - \sqrt{3}u_{Y_2 0} + L\theta_{X_2 0} - \sqrt{2L}\theta_{Z_2 0})}{6k_b} \\ \theta_{Y_2 0} - \frac{Lk_s(-\sqrt{2L}\bar{\epsilon}_{X_2 X_2} + L\bar{\epsilon}_{X_2 Z_2} + \sqrt{2L}\bar{\epsilon}_{Z_2 Z_2} + \sqrt{3}u_{X_2 0} - \sqrt{6}u_{Z_2 0} + 3L\theta_{Y_2 0})}{6k_b} \\ \theta_{Z_2 0} + \frac{Lk_s(2L\bar{\epsilon}_{X_2 Y_2} + \sqrt{2L}\bar{\epsilon}_{Y_2 Z_2} - \sqrt{6}u_{Y_2 0} + \sqrt{2L}\theta_{X_2 0} - 2L\theta_{Z_2 0})}{6k_b} \end{Bmatrix}, \quad (98)$$

$$\begin{Bmatrix} \theta_{X_2 4} \\ \theta_{Y_2 4} \\ \theta_{Z_2 4} \end{Bmatrix} = \begin{Bmatrix} \theta_{X_2 0} - \frac{Lk_s(-\sqrt{2L}\bar{\epsilon}_{X_2 Y_2} + L\bar{\epsilon}_{Y_2 Z_2} - \sqrt{3}u_{Y_2 0} + L\theta_{X_2 0} + \sqrt{2L}\theta_{Z_2 0})}{6k_b} \\ \theta_{Y_2 0} - \frac{Lk_s(\sqrt{2L}\bar{\epsilon}_{X_2 X_2} + L\bar{\epsilon}_{X_2 Z_2} - \sqrt{2L}\bar{\epsilon}_{Z_2 Z_2} + \sqrt{3}u_{X_2 0} + \sqrt{6}u_{Z_2 0} + 3L\theta_{Y_2 0})}{6k_b} \\ \theta_{Z_2 0} - \frac{Lk_s(-2L\bar{\epsilon}_{X_2 Y_2} + \sqrt{2L}\bar{\epsilon}_{Y_2 Z_2} - \sqrt{6}u_{Y_2 0} + \sqrt{2L}\theta_{X_2 0} + 2L\theta_{Z_2 0})}{6k_b} \end{Bmatrix}. \quad (99)$$

Substituting Equations (1), (2), (7), (9), (12), (13), (92), (94) and (96)–(99) into the equilibrium equations at the interior nodes listed in Equation (31) gives the displacement and rotation components at the central node as

$$\begin{Bmatrix} u_{X_2 0} \\ u_{Y_2 0} \\ u_{Z_2 0} \\ \theta_{X_2 0} \\ \theta_{Y_2 0} \\ \theta_{Z_2 0} \end{Bmatrix} = \begin{Bmatrix} \sqrt{3}\left(-\frac{1}{3} + \frac{2k_a k_b}{2k_a k_b + 4k_b k_s - L^2 k_s^2}\right) \bar{\epsilon}_{X_2 Z_2} L \\ \sqrt{3}\left(\frac{1}{3} - \frac{2k_a k_b}{2k_a k_b + 4k_b k_s - L^2 k_s^2}\right) \bar{\epsilon}_{Y_2 Z_2} L \\ \sqrt{3}\left(-\frac{1}{6} + \frac{k_a k_b}{2k_a k_b + 4k_b k_s - L^2 k_s^2}\right) (\bar{\epsilon}_{X_2 X_2} - \bar{\epsilon}_{Y_2 Y_2}) L \\ 0 \\ 0 \\ 0 \end{Bmatrix}. \quad (100)$$

It follows from Equations (1), (2), (7), (9), (15), (25), (29), (92), (94), (96)–(99) and (100) that the strain energy density function in this case is given by

$$\begin{aligned} u &= \frac{\sqrt{3}}{8} \left[\frac{k_a^2 + 7k_a k_s + k_s^2}{3L(k_a + 2k_s)} - \frac{Lk_s^2}{24k_b} - \frac{3Lk_a^2 k_s^2}{4(k_a + 2k_s)(2k_a k_b + 4k_b k_s - L^2 k_s^2)} \right] (\bar{\epsilon}_{X_2 X_2}^2 + \bar{\epsilon}_{Y_2 Y_2}^2) \\ &+ \frac{\sqrt{3}}{24L} \left(k_a + 2k_s - \frac{L^2 k_s^2}{2k_b} \right) \bar{\epsilon}_{ZZ}^2 + \frac{3\sqrt{3}k_a k_s}{8(k_a + 2k_s)} \left(\frac{2}{L} - \frac{Lk_a k_s}{2k_a k_b + 4k_b k_s - L^2 k_s^2} \right) (\bar{\epsilon}_{X_2 Z_2}^2 + \bar{\epsilon}_{Y_2 Z_2}^2) \\ &+ \frac{\sqrt{3}}{8L} \left(2k_s - \frac{L^2 k_s^2}{2k_b} \right) \bar{\epsilon}_{XY}^2 + \frac{\sqrt{3}}{12L} \left(k_a - k_s + \frac{L^2 k_s^2}{4k_b} \right) (\bar{\epsilon}_{X_2 X_2} \bar{\epsilon}_{Z_2 Z_2} + \bar{\epsilon}_{Y_2 Y_2} \bar{\epsilon}_{Z_2 Z_2}) \\ &+ \frac{\sqrt{3}}{8} \left[\frac{2(k_a - k_s)^2}{3L(k_a + 2k_s)} - \frac{Lk_s^2}{12k_b} + \frac{3Lk_a^2 k_s^2}{2(k_a + 2k_s)(2k_a k_b + 4k_b k_s - L^2 k_s^2)} \right] \bar{\epsilon}_{X_2 X_2} \bar{\epsilon}_{Y_2 Y_2}. \end{aligned} \quad (101)$$

Clearly, there is no unknown kinematic variable in Equation (101).

Finally, from Equations (32) and (101) the effective stiffness matrix $\bar{\mathbf{C}}^{(2)}$ for the pentamode metamaterial based on the representative cell in orientation # 2 shown in Figure 8b can be obtained as the coefficient matrix of the following constitutive equations:

$$\begin{Bmatrix} \bar{\sigma}_{X_2 X_2} \\ \bar{\sigma}_{Y_2 Y_2} \\ \bar{\sigma}_{Z_2 Z_2} \\ \bar{\sigma}_{Y_2 Z_2} \\ \bar{\sigma}_{X_2 Z_2} \\ \bar{\sigma}_{X_2 Y_2} \end{Bmatrix} = \begin{bmatrix} \chi_{1M}^{(2)} & \chi_{2M}^{(2)} & \chi_{3M}^{(2)} & 0 & 0 & 0 \\ \chi_{2M}^{(2)} & \chi_{1M}^{(2)} & \chi_{3M}^{(2)} & 0 & 0 & 0 \\ \chi_{3M}^{(2)} & \chi_{3M}^{(2)} & \chi_{4M}^{(2)} & 0 & 0 & 0 \\ 0 & 0 & 0 & \chi_{6M}^{(2)} & 0 & 0 \\ 0 & 0 & 0 & 0 & \chi_{6M}^{(2)} & 0 \\ 0 & 0 & 0 & 0 & 0 & \chi_{5M}^{(2)} \end{bmatrix} \begin{Bmatrix} \bar{\epsilon}_{X_2 X_2} \\ \bar{\epsilon}_{Y_2 Y_2} \\ \bar{\epsilon}_{Z_2 Z_2} \\ \bar{\epsilon}_{Y_2 Z_2} \\ \bar{\epsilon}_{X_2 Z_2} \\ \bar{\epsilon}_{X_2 Y_2} \end{Bmatrix} = \bar{\mathbf{C}}^{(2)} \begin{Bmatrix} \bar{\epsilon}_{X_2 X_2} \\ \bar{\epsilon}_{Y_2 Y_2} \\ \bar{\epsilon}_{Z_2 Z_2} \\ \bar{\epsilon}_{Y_2 Z_2} \\ \bar{\epsilon}_{X_2 Z_2} \\ \bar{\epsilon}_{X_2 Y_2} \end{Bmatrix}, \quad (102)$$

where

$$\begin{aligned}\chi_{1M}^{(2)} &= \frac{\sqrt{3}(26k_a k_b + 4k_b k_s - L^2 k_s^2)}{96Lk_b} - \frac{3\sqrt{3}k_a^2 k_b}{8L(2k_a k_b + 4k_b k_s - L^2 k_s^2)}, \\ \chi_{2M}^{(2)} &= \frac{\sqrt{3}(4k_a k_b - 4k_b k_s + L^2 k_s^2)^2}{96Lk_b(2k_a k_b + 4k_b k_s - L^2 k_s^2)}, \quad \chi_{3M}^{(2)} = \frac{\sqrt{3}(k_a - k_s)}{12L} + \frac{\sqrt{3}Lk_s^2}{48k_b}, \\ \chi_{4M}^{(2)} &= \frac{\sqrt{3}(k_a + 2k_s)}{12L} - \frac{\sqrt{3}Lk_s^2}{24k_b}, \quad \chi_{5M}^{(2)} = \frac{\sqrt{3}k_s}{2L} - \frac{\sqrt{3}Lk_s^2}{8k_b}, \\ \chi_{6M}^{(2)} &= \frac{3\sqrt{3}k_a k_s(4k_b - L^2 k_s)}{4L(2k_a k_b + 4k_b k_s - L^2 k_s^2)}.\end{aligned}\quad (103)$$

Clearly, Equations (102) and (103) show that the stiffness matrix $\bar{\mathbf{C}}^{(2)}$ of the pentamode metamaterial obtained using the representative cell in orientation # 2 does not exhibit the cubic symmetry. This differs from the stiffness matrix $\bar{\mathbf{C}}^{(1)}$ derived in Equations (83) and (84) based on the representative cell in orientation # 1.

The effective compliance matrix $\bar{\mathbf{S}}^{(2)} = [\bar{\mathbf{C}}^{(2)}]^{-1}$ based on the representative cell in orientation # 2 can then be readily obtained from Equations (102) and (103) as

$$\bar{\mathbf{S}}^{(2)} = \begin{bmatrix} \zeta_{1M}^{(2)} & 0 & \zeta_{2M}^{(2)} & 0 & 0 & 0 \\ 0 & \zeta_{1M}^{(2)} & \zeta_{2M}^{(2)} & 0 & 0 & 0 \\ \zeta_{2M}^{(2)} & \zeta_{2M}^{(2)} & \zeta_{3M}^{(2)} & 0 & 0 & 0 \\ 0 & 0 & 0 & \zeta_{4M}^{(2)} & 0 & 0 \\ 0 & 0 & 0 & 0 & \zeta_{4M}^{(2)} & 0 \\ 0 & 0 & 0 & 0 & 0 & \zeta_{5M}^{(2)} \end{bmatrix}, \quad (104)$$

where

$$\begin{aligned}\zeta_{1M}^{(2)} &= \frac{8\sqrt{3}L}{9k_a} + \frac{16\sqrt{3}Lk_b}{9k_s(4k_b - L^2 k_s)}, \quad \zeta_{2M}^{(2)} = \frac{4\sqrt{3}L}{9k_a} - \frac{16\sqrt{3}Lk_b}{9k_s(4k_b - L^2 k_s)}, \\ \zeta_{3M}^{(2)} &= \frac{4\sqrt{3}L}{9k_a} + \frac{32\sqrt{3}Lk_b}{9k_s(4k_b - L^2 k_s)}, \quad \zeta_{4M}^{(2)} = \frac{4\sqrt{3}L}{9k_a} + \frac{8\sqrt{3}Lk_b}{9k_s(4k_b - L^2 k_s)}, \\ \zeta_{5M}^{(2)} &= \frac{8\sqrt{3}Lk_b}{3k_s(4k_b - L^2 k_s)}.\end{aligned}\quad (105)$$

It can be readily verified that the effective stiffness and compliance matrices obtained in Equations (102) and (103) and Equations (104) and (105) from the representative cell in orientation # 2 shown in Figure 8b can be reproduced from the effective stiffness and compliance matrices derived in Equations (83) and (84) and Equations (85) and (86) based on the representative cell in orientation # 1 displayed in Figure 8a by using a coordinate transformation, as shown next.

When the coordinate system # 1 is rotated by an angle of θ about the common Z-axis to the coordinate system # 2, the effective stiffness and compliance matrices satisfy the following transformation relations [51]

$$\bar{\mathbf{C}}_V^{(2)} = \mathbf{R}\bar{\mathbf{C}}_V^{(1)}\mathbf{R}^T, \quad \bar{\mathbf{S}}_V^{(2)} = \mathbf{R}^{-T}\bar{\mathbf{S}}_V^{(1)}\mathbf{R}^{-1}, \quad (106)$$

$$\mathbf{R} = \begin{bmatrix} \cos^2 \theta & \sin^2 \theta & 0 & 0 & 0 & 2 \cos \theta \sin \theta \\ \sin^2 \theta & \cos^2 \theta & 0 & 0 & 0 & -2 \cos \theta \sin \theta \\ 0 & 0 & 1 & 0 & 0 & 0 \\ 0 & 0 & 0 & \cos \theta & -\sin \theta & 0 \\ 0 & 0 & 0 & \sin \theta & \cos \theta & 0 \\ -\cos \theta \sin \theta & \cos \theta \sin \theta & 0 & 0 & 0 & \cos^2 \theta - \sin^2 \theta \end{bmatrix}, \quad (107)$$

where the subscript "V" denotes the matrix based on $\boldsymbol{\varepsilon} = [\varepsilon_{11} \quad \varepsilon_{22} \quad \varepsilon_{33} \quad 2\varepsilon_{23} \quad 2\varepsilon_{31} \quad 2\varepsilon_{12}]^T$ (the Voigt notation), and the superscripts "(1)" and "(2)" refer to the effective stiffness or compliance matrix obtained using the coordinate systems adopted in the representative

cells in orientations # 1 and # 2, respectively. By setting $\theta = -45^\circ$ (i.e., clockwise rotation from the orientation # 1 to the orientation # 2) and noting the difference between the $\bar{\mathbf{C}}$ and $\bar{\mathbf{S}}$ matrices obtained earlier in this section based on $\boldsymbol{\varepsilon} = [\varepsilon_{11} \ \varepsilon_{22} \ \varepsilon_{33} \ \varepsilon_{23} \ \varepsilon_{31} \ \varepsilon_{12}]^T$ and the $\bar{\mathbf{C}}_V$ and $\bar{\mathbf{S}}_V$ matrices, Equations (106) and (107) will lead to the matrices $\bar{\mathbf{C}}^{(2)}$ and $\bar{\mathbf{S}}^{(2)}$ in Equations (102) and (104) for orientation # 2 from $\bar{\mathbf{C}}^{(1)}$ and $\bar{\mathbf{S}}^{(1)}$ in Equations (83) and (85) for orientation # 1.

Similarly, it can be readily shown that the engineering constants determined by substituting $\bar{s}_{11}^{(2)}$, $\bar{s}_{12}^{(2)}$ and $\bar{s}_{66}^{(2)}$ obtained from Equations (106) and (107) into Equation (87) are the same as those given by Equation (91).

These verify and support the newly proposed homogenization approach.

3.2.3. Homogenization with Periodicity Constraints

Periodicity constraints are considered in homogenizing the pentamode metamaterial shown in Figure 10 using the method proposed in Section 2.4. As discussed earlier, the unit cell is repetitive along three directions which are not mutually perpendicular to each other.

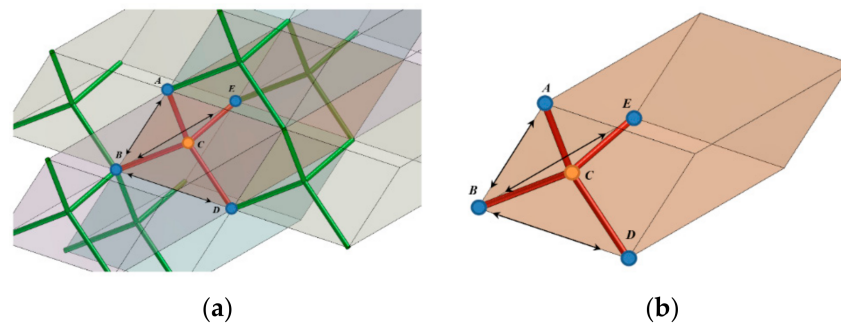


Figure 10. Periodic pentamode metamaterial: (a) microstructure; (b) diamond-shaped unit cell.

From Figure 10, it is seen that the pentamode material can be generated by repeating the diamond-shaped unit cell along the directions $\overset{\leftrightarrow}{BA}$, $\overset{\leftrightarrow}{BD}$ and $\overset{\leftrightarrow}{BE}$. This indicates that nodes A , D and E on the cell boundary can each form a periodic pair with node B . That is, the four boundary nodes belong to one periodic pair. From Equations (35) and (36), it follows that for the periodic pair of the four boundary nodes A , B , D and E based on the representative cell in orientation # 1,

$$\begin{pmatrix} u_{X_1 1}^* \\ u_{Y_1 1}^* \\ u_{Z_1 1}^* \\ \theta_{X_1 1}^* \\ \theta_{Y_1 1}^* \\ \theta_{Z_1 1}^* \end{pmatrix} = \begin{pmatrix} u_{X_1 2}^* \\ u_{Y_1 2}^* \\ u_{Z_1 2}^* \\ \theta_{X_1 2}^* \\ \theta_{Y_1 2}^* \\ \theta_{Z_1 2}^* \end{pmatrix} = \begin{pmatrix} u_{X_1 3}^* \\ u_{Y_1 3}^* \\ u_{Z_1 3}^* \\ \theta_{X_1 3}^* \\ \theta_{Y_1 3}^* \\ \theta_{Z_1 3}^* \end{pmatrix} = \begin{pmatrix} u_{X_1 4}^* \\ u_{Y_1 4}^* \\ u_{Z_1 4}^* \\ \theta_{X_1 4}^* \\ \theta_{Y_1 4}^* \\ \theta_{Z_1 4}^* \end{pmatrix} = \begin{pmatrix} u_{X_1}^* \\ u_{Y_1}^* \\ u_{Z_1}^* \\ \theta_{X_1}^* \\ \theta_{Y_1}^* \\ \theta_{Z_1}^* \end{pmatrix}, \begin{pmatrix} F_{X_1 1} + F_{X_1 2} + F_{X_1 3} + F_{X_1 4} \\ F_{Y_1 1} + F_{Y_1 2} + F_{Y_1 3} + F_{Y_1 4} \\ F_{Z_1 1} + F_{Z_1 2} + F_{Z_1 3} + F_{Z_1 4} \\ M_{X_1 1} + M_{X_1 2} + M_{X_1 3} + M_{X_1 4} \\ M_{Y_1 1} + M_{Y_1 2} + M_{Y_1 3} + M_{Y_1 4} \\ M_{Z_1 1} + M_{Z_1 2} + M_{Z_1 3} + M_{Z_1 4} \end{pmatrix} = \begin{pmatrix} 0 \\ 0 \\ 0 \\ 0 \\ 0 \\ 0 \end{pmatrix}, \quad (108)$$

and for the periodic pair of the four boundary nodes based on the representative cell in orientation # 2,

$$\begin{pmatrix} u_{X_2 1}^* \\ u_{Y_2 1}^* \\ u_{Z_2 1}^* \\ \theta_{X_2 1}^* \\ \theta_{Y_2 1}^* \\ \theta_{Z_2 1}^* \end{pmatrix} = \begin{pmatrix} u_{X_2 2}^* \\ u_{Y_2 2}^* \\ u_{Z_2 2}^* \\ \theta_{X_2 2}^* \\ \theta_{Y_2 2}^* \\ \theta_{Z_2 2}^* \end{pmatrix} = \begin{pmatrix} u_{X_2 3}^* \\ u_{Y_2 3}^* \\ u_{Z_2 3}^* \\ \theta_{X_2 3}^* \\ \theta_{Y_2 3}^* \\ \theta_{Z_2 3}^* \end{pmatrix} = \begin{pmatrix} u_{X_2 4}^* \\ u_{Y_2 4}^* \\ u_{Z_2 4}^* \\ \theta_{X_2 4}^* \\ \theta_{Y_2 4}^* \\ \theta_{Z_2 4}^* \end{pmatrix} = \begin{pmatrix} u_{X_2}^* \\ u_{Y_2}^* \\ u_{Z_2}^* \\ \theta_{X_2}^* \\ \theta_{Y_2}^* \\ \theta_{Z_2}^* \end{pmatrix}, \begin{pmatrix} F_{X_2 1} + F_{X_2 2} + F_{X_2 3} + F_{X_2 4} \\ F_{Y_2 1} + F_{Y_2 2} + F_{Y_2 3} + F_{Y_2 4} \\ F_{Z_2 1} + F_{Z_2 2} + F_{Z_2 3} + F_{Z_2 4} \\ M_{X_2 1} + M_{X_2 2} + M_{X_2 3} + M_{X_2 4} \\ M_{Y_2 1} + M_{Y_2 2} + M_{Y_2 3} + M_{Y_2 4} \\ M_{Z_2 1} + M_{Z_2 2} + M_{Z_2 3} + M_{Z_2 4} \end{pmatrix} = \begin{pmatrix} 0 \\ 0 \\ 0 \\ 0 \\ 0 \\ 0 \end{pmatrix}. \quad (109)$$

Homogenization Based on the First Representative Cell with Periodicity Constraints

For the representative cell shown in Figure 8a, the displacement and rotation components at the four boundary nodes can be obtained from Equations (18), (37), (74) and (108) as

$$\begin{cases} u_{X11} \\ u_{Y11} \\ u_{Z11} \end{cases} = -\frac{L}{\sqrt{3}} \begin{cases} \bar{\varepsilon}_{X1X1} + \bar{\varepsilon}_{X1Y1} + \bar{\varepsilon}_{X1Z1} \\ \bar{\varepsilon}_{X1Y1} + \bar{\varepsilon}_{Y1Y1} + \bar{\varepsilon}_{Y1Z1} \\ \bar{\varepsilon}_{X1Z1} + \bar{\varepsilon}_{Y1Z1} + \bar{\varepsilon}_{Z1Z1} \end{cases} + \begin{cases} u_{X1}^* \\ u_{Y1}^* \\ u_{Z1}^* \end{cases}, \quad \begin{cases} u_{X12} \\ u_{Y12} \\ u_{Z12} \end{cases} = \frac{L}{\sqrt{3}} \begin{cases} \bar{\varepsilon}_{X1X1} + \bar{\varepsilon}_{X1Y1} - \bar{\varepsilon}_{X1Z1} \\ \bar{\varepsilon}_{X1Y1} + \bar{\varepsilon}_{Y1Y1} - \bar{\varepsilon}_{Y1Z1} \\ \bar{\varepsilon}_{X1Z1} + \bar{\varepsilon}_{Y1Z1} - \bar{\varepsilon}_{Z1Z1} \end{cases} + \begin{cases} u_{X1}^* \\ u_{Y1}^* \\ u_{Z1}^* \end{cases}, \quad (110)$$

$$\begin{cases} u_{X13} \\ u_{Y13} \\ u_{Z13} \end{cases} = \frac{L}{\sqrt{3}} \begin{cases} \bar{\varepsilon}_{X1X1} - \bar{\varepsilon}_{X1Y1} + \bar{\varepsilon}_{X1Z1} \\ \bar{\varepsilon}_{X1Y1} - \bar{\varepsilon}_{Y1Y1} + \bar{\varepsilon}_{Y1Z1} \\ \bar{\varepsilon}_{X1Z1} - \bar{\varepsilon}_{Y1Z1} + \bar{\varepsilon}_{Z1Z1} \end{cases} + \begin{cases} u_{X1}^* \\ u_{Y1}^* \\ u_{Z1}^* \end{cases}, \quad \begin{cases} u_{X14} \\ u_{Y14} \\ u_{Z14} \end{cases} = \frac{L}{\sqrt{3}} \begin{cases} -\bar{\varepsilon}_{X1X1} + \bar{\varepsilon}_{X1Y1} + \bar{\varepsilon}_{X1Z1} \\ -\bar{\varepsilon}_{X1Y1} + \bar{\varepsilon}_{Y1Y1} + \bar{\varepsilon}_{Y1Z1} \\ -\bar{\varepsilon}_{X1Z1} + \bar{\varepsilon}_{Y1Z1} + \bar{\varepsilon}_{Z1Z1} \end{cases} + \begin{cases} u_{X1}^* \\ u_{Y1}^* \\ u_{Z1}^* \end{cases}.$$

$$\begin{cases} \theta_{X11} \\ \theta_{Y11} \\ \theta_{Z11} \end{cases} = \begin{cases} \theta_{X12} \\ \theta_{Y12} \\ \theta_{Z12} \end{cases} = \begin{cases} \theta_{X13} \\ \theta_{Y13} \\ \theta_{Z13} \end{cases} = \begin{cases} \theta_{X14} \\ \theta_{Y14} \\ \theta_{Z14} \end{cases} = \begin{cases} \theta_{X1}^* \\ \theta_{Y1}^* \\ \theta_{Z1}^* \end{cases}. \quad (111)$$

Using Equations (1), (2), (7), (9), (12), (13), (73), (110) and (111) in the anti-periodicity conditions listed in Equation (108) yields the periodic parts of the displacement and rotation at the four boundary nodes as

$$\begin{cases} u_{X1}^* \\ u_{Y1}^* \\ u_{Z1}^* \end{cases} = \begin{cases} u_{X1o} - \left(\frac{\sqrt{3}L}{3} - \frac{\sqrt{3}Lk_a}{k_a+2k_s} \right) \bar{\varepsilon}_{Y1Z1} \\ u_{Y1o} - \left(\frac{\sqrt{3}L}{3} - \frac{\sqrt{3}Lk_a}{k_a+2k_s} \right) \bar{\varepsilon}_{X1Z1} \\ u_{Z1o} - \left(\frac{\sqrt{3}L}{3} - \frac{\sqrt{3}Lk_a}{k_a+2k_s} \right) \bar{\varepsilon}_{X1Y1} \end{cases}, \quad \begin{cases} \theta_{X1}^* \\ \theta_{Y1}^* \\ \theta_{Z1}^* \end{cases} = \begin{cases} \left(1 - \frac{L^2k_s}{2k_b+k_t} \right) \theta_{X1o} \\ \left(1 - \frac{L^2k_s}{2k_b+k_t} \right) \theta_{Y1o} \\ \left(1 - \frac{L^2k_s}{2k_b+k_t} \right) \theta_{Z1o} \end{cases}. \quad (112)$$

Next, applying the equilibrium conditions at the central node o (an interior node) listed in Equation (31) leads to, after using Equations (1), (2), (7), (9), (12), (13), (73) and (110)–(112) and setting $u_{Xo} = u_{Yo} = u_{Zo} = 0$ (i.e., no rigid-body displacement enforced at the central node o),

$$\theta_{X1o} = \theta_{Y1o} = \theta_{Z1o} = 0. \quad (113)$$

From Equations (1), (2), (9), (15), (25), (29), (73) and (110)–(113), it follows that the strain energy density function in this case is given by

$$u = \frac{\sqrt{3}(k_a+2k_s)}{24L} \left(\bar{\varepsilon}_{X1X1}^2 + \bar{\varepsilon}_{Y1Y1}^2 + \bar{\varepsilon}_{Z1Z1}^2 \right) + \frac{3\sqrt{3}k_s k_a}{4L(k_a+2k_s)} \left(\bar{\varepsilon}_{X1Y1}^2 + \bar{\varepsilon}_{X1Z1}^2 + \bar{\varepsilon}_{Y1Z1}^2 \right) + \frac{\sqrt{3}(k_a-k_s)}{12L} \left(\bar{\varepsilon}_{X1X1} \bar{\varepsilon}_{Y1Y1} + \bar{\varepsilon}_{X1X1} \bar{\varepsilon}_{Z1Z1} + \bar{\varepsilon}_{Y1Y1} \bar{\varepsilon}_{Z1Z1} \right), \quad (114)$$

which no longer depends on the strut bending stiffness k_b , unlike that obtained in Equation (82) without the periodicity constraints. This is consistent with what is observed from comparing the 2-D cases with and without the periodic constraints in Section 3.1.

Then, the effective stiffness matrix $\bar{\mathbf{C}}_p^{(1)}$ for the pentamode metamaterial based on the representative cell in orientation # 1 shown in Figure 8a with the periodic boundary conditions listed in Equations (110)–(112) can be obtained from Equations (32) and (114) as

$$\begin{cases} \bar{\sigma}_{X1X1} \\ \bar{\sigma}_{Y1Y1} \\ \bar{\sigma}_{Z1Z1} \\ \bar{\sigma}_{Y1Z1} \\ \bar{\sigma}_{X1Z1} \\ \bar{\sigma}_{X1Y1} \end{cases} = \begin{bmatrix} \chi_{1P}^{(1)} & \chi_{2P}^{(1)} & \chi_{2P}^{(1)} & 0 & 0 & 0 \\ \chi_{2P}^{(1)} & \chi_{1P}^{(1)} & \chi_{2P}^{(1)} & 0 & 0 & 0 \\ \chi_{2P}^{(1)} & \chi_{2P}^{(1)} & \chi_{1P}^{(1)} & 0 & 0 & 0 \\ 0 & 0 & 0 & \chi_{3P}^{(1)} & 0 & 0 \\ 0 & 0 & 0 & 0 & \chi_{3P}^{(1)} & 0 \\ 0 & 0 & 0 & 0 & 0 & \chi_{3P}^{(1)} \end{bmatrix} \begin{cases} \bar{\varepsilon}_{X1X1} \\ \bar{\varepsilon}_{Y1Y1} \\ \bar{\varepsilon}_{Z1Z1} \\ \bar{\varepsilon}_{Y1Z1} \\ \bar{\varepsilon}_{X1Z1} \\ \bar{\varepsilon}_{X1Y1} \end{cases} = \bar{\mathbf{C}}_p^{(1)} \begin{cases} \bar{\varepsilon}_{X1X1} \\ \bar{\varepsilon}_{Y1Y1} \\ \bar{\varepsilon}_{Z1Z1} \\ \bar{\varepsilon}_{Y1Z1} \\ \bar{\varepsilon}_{X1Z1} \\ \bar{\varepsilon}_{X1Y1} \end{cases}, \quad (115)$$

where

$$\chi_{1P}^{(1)} = \frac{\sqrt{3}(k_a + 2k_s)}{12L}, \quad \chi_{2P}^{(1)} = \frac{\sqrt{3}(k_a - k_s)}{12L}, \quad \chi_{3P}^{(1)} = \frac{3\sqrt{3}k_a k_s}{2L(k_a + 2k_s)}. \quad (116)$$

Clearly, Equations (115) and (116) show that the pentamode metamaterial with the periodicity constraints based on the representative cell in orientation # 1 exhibits the cubic symmetry, which is the same as what is observed from Equations (83) and (84) for the same representative cell and orientation but without the periodicity constraints. In addition, it is seen from Equations (115) and (116) that the effective stiffness components do not depend on the strut bending stiffness k_b , which differs from those given in Equations (83) and (84) for the pentamode metamaterial without imposing the periodicity constraints.

The compliance matrix $\bar{\mathbf{S}}_P^{(1)} = [\bar{\mathbf{C}}_P^{(1)}]^{-1}$ based on the representative cell in orientation # 1 with the periodicity constraints can then be readily determined as

$$\bar{\mathbf{S}}_P^{(1)} = \begin{bmatrix} \zeta_{1P}^{(1)} & \zeta_{2P}^{(1)} & \zeta_{2P}^{(1)} & 0 & 0 & 0 \\ \zeta_{2P}^{(1)} & \zeta_{1P}^{(1)} & \zeta_{2P}^{(1)} & 0 & 0 & 0 \\ \zeta_{2P}^{(1)} & \zeta_{2P}^{(1)} & \zeta_{1P}^{(1)} & 0 & 0 & 0 \\ 0 & 0 & 0 & \zeta_{3P}^{(1)} & 0 & 0 \\ 0 & 0 & 0 & 0 & \zeta_{3P}^{(1)} & 0 \\ 0 & 0 & 0 & 0 & 0 & \zeta_{3P}^{(1)} \end{bmatrix}, \quad (117)$$

where

$$\zeta_{1P}^{(1)} = \frac{4\sqrt{3}L}{9} \left(\frac{1}{k_a} + \frac{2}{k_s} \right), \quad \zeta_{2P}^{(1)} = \frac{4\sqrt{3}L}{9} \left(\frac{1}{k_a} - \frac{1}{k_s} \right), \quad \zeta_{3P}^{(1)} = \frac{4\sqrt{3}L}{9} \left(\frac{1}{k_a} + \frac{1}{2k_s} \right). \quad (118)$$

Homogenization Based on the Second Representative Cell with Periodicity Constraints

For the representative cell in orientation # 2 shown in Figure 8b, the displacement and rotation vectors at the four boundary nodes can be obtained from Equations (18), (37), (93) and (109) as

$$\begin{aligned} \begin{Bmatrix} u_{X_21} \\ u_{Y_21} \\ u_{Z_21} \end{Bmatrix} &= -\frac{L}{\sqrt{3}} \begin{Bmatrix} \sqrt{2}\bar{\epsilon}_{X_2Y_2} + \bar{\epsilon}_{X_2Z_2} \\ \sqrt{2}\bar{\epsilon}_{Y_2Y_2} + \bar{\epsilon}_{Y_2Z_2} \\ \sqrt{2}\bar{\epsilon}_{Y_2Z_2} + \bar{\epsilon}_{Z_2Z_2} \end{Bmatrix} + \begin{Bmatrix} u_{X_2}^* \\ u_{Y_2}^* \\ u_{Z_2}^* \end{Bmatrix}, & \begin{Bmatrix} u_{X_22} \\ u_{Y_22} \\ u_{Z_22} \end{Bmatrix} &= \frac{L}{\sqrt{3}} \begin{Bmatrix} \sqrt{2}\bar{\epsilon}_{X_2Y_2} - \bar{\epsilon}_{X_2Z_2} \\ \sqrt{2}\bar{\epsilon}_{Y_2Y_2} - \bar{\epsilon}_{Y_2Z_2} \\ \sqrt{2}\bar{\epsilon}_{Y_2Z_2} - \bar{\epsilon}_{Z_2Z_2} \end{Bmatrix} + \begin{Bmatrix} u_{X_2}^* \\ u_{Y_2}^* \\ u_{Z_2}^* \end{Bmatrix}, \\ \begin{Bmatrix} u_{X_23} \\ u_{Y_23} \\ u_{Z_23} \end{Bmatrix} &= \frac{L}{\sqrt{3}} \begin{Bmatrix} \sqrt{2}\bar{\epsilon}_{X_2X_2} + \bar{\epsilon}_{X_2Z_2} \\ \sqrt{2}\bar{\epsilon}_{X_2Y_2} + \bar{\epsilon}_{Y_2Z_2} \\ \sqrt{2}\bar{\epsilon}_{X_2Z_2} + \bar{\epsilon}_{Z_2Z_2} \end{Bmatrix} + \begin{Bmatrix} u_{X_2}^* \\ u_{Y_2}^* \\ u_{Z_2}^* \end{Bmatrix}, & \begin{Bmatrix} u_{X_24} \\ u_{Y_24} \\ u_{Z_24} \end{Bmatrix} &= \frac{L}{\sqrt{3}} \begin{Bmatrix} -\sqrt{2}\bar{\epsilon}_{X_2X_2} + \bar{\epsilon}_{X_2Z_2} \\ -\sqrt{2}\bar{\epsilon}_{X_2Y_2} + \bar{\epsilon}_{Y_2Z_2} \\ -\sqrt{2}\bar{\epsilon}_{X_2Z_2} + \bar{\epsilon}_{Z_2Z_2} \end{Bmatrix} + \begin{Bmatrix} u_{X_2}^* \\ u_{Y_2}^* \\ u_{Z_2}^* \end{Bmatrix}, \end{aligned} \quad (119)$$

$$\begin{Bmatrix} \theta_{X_21} \\ \theta_{Y_21} \\ \theta_{Z_21} \end{Bmatrix} = \begin{Bmatrix} \theta_{X_22} \\ \theta_{Y_22} \\ \theta_{Z_22} \end{Bmatrix} = \begin{Bmatrix} \theta_{X_23} \\ \theta_{Y_23} \\ \theta_{Z_23} \end{Bmatrix} = \begin{Bmatrix} \theta_{X_24} \\ \theta_{Y_24} \\ \theta_{Z_24} \end{Bmatrix} = \begin{Bmatrix} \theta_{X_2}^* \\ \theta_{Y_2}^* \\ \theta_{Z_2}^* \end{Bmatrix}. \quad (120)$$

Using Equations (1), (2), (7), (9), (12), (13), (92), (119) and (120) in Equation (109) gives the periodic parts of the displacement and rotation components at the four boundary nodes as

$$\begin{Bmatrix} u_{X_2}^* \\ u_{Y_2}^* \\ u_{Z_2}^* \end{Bmatrix} = \begin{Bmatrix} u_{X_{20}} + \frac{2\sqrt{3}}{3} \frac{k_s - k_a}{k_a + 2k_s} \bar{\epsilon}_{X_2Z_2} L \\ u_{Y_{20}} - \frac{2\sqrt{3}}{3} \frac{k_s - k_a}{k_a + 2k_s} \bar{\epsilon}_{Y_2Z_2} L \\ u_{Z_{20}} + \frac{\sqrt{3}}{3} \frac{k_s - k_a}{k_a + 2k_s} (\bar{\epsilon}_{X_2X_2} - \bar{\epsilon}_{Y_2Y_2}) L \end{Bmatrix}, \quad \begin{Bmatrix} \theta_{X_2}^* \\ \theta_{Y_2}^* \\ \theta_{Z_2}^* \end{Bmatrix} = \begin{Bmatrix} \left(1 - \frac{L^2 k_s}{2k_b + k_t}\right) \theta_{X_{20}} \\ \left(1 - \frac{L^2 k_s}{2k_b + k_t}\right) \theta_{Y_{20}} \\ \left(1 - \frac{L^2 k_s}{2k_b + k_t}\right) \theta_{Z_{20}} \end{Bmatrix}. \quad (121)$$

Next, applying the equilibrium conditions at the central node o (an interior node) listed in Equation (31) results in, after using Equations (1), (2), (7), (9), (12), (13), (92) and (119)–(121) and setting $u_{X_0} = u_{Y_0} = u_{Z_0} = 0$ (i.e., no rigid-body displacement enforced at the central node o),

$$\theta_{X_{2o}} = \theta_{Y_{2o}} = \theta_{Z_{2o}} = 0. \tag{122}$$

From Equations (1), (2), (9), (15), (25), (29), (92) and (119)–(122), the strain energy density function in this case can be obtained as

$$u = \frac{\sqrt{3}}{24L} \frac{k_a^2 + 7k_a k_s + k_s^2}{k_a + 2k_s} (\bar{\epsilon}_{X_2 X_2}^2 + \bar{\epsilon}_{Y_2 Y_2}^2) + \frac{\sqrt{3}(k_a + 2k_s)}{24L} \bar{\epsilon}_{Z_2 Z_2}^2 + \frac{\sqrt{3}}{12L} \frac{(k_a - k_s)^2}{k_a + 2k_s} \bar{\epsilon}_{X_2 X_2} \bar{\epsilon}_{Y_2 Y_2} + \frac{\sqrt{3}(k_a - k_s)}{12L} (\bar{\epsilon}_{X_2 X_2} \bar{\epsilon}_{Z_2 Z_2} + \bar{\epsilon}_{Y_2 Y_2} \bar{\epsilon}_{Z_2 Z_2}) + \frac{3\sqrt{3}}{4L} \frac{k_s k_a}{k_a + 2k_s} (\bar{\epsilon}_{Y_2 Z_2}^2 + \bar{\epsilon}_{X_2 Z_2}^2) + \frac{\sqrt{3}k_s}{4L} \bar{\epsilon}_{X_2 Y_2}^2. \tag{123}$$

Clearly, this strain energy density function does not depend on the strut bending stiffness k_b , which is different from that obtained in Equation (101) based on the representative cell shown in Figure 8b without using the periodicity constraints. This is similar to what is observed from comparing Equations (114) and (82), which are based on the representative cell shown in Figure 8a with and without the periodicity constraints.

Then, it follows from Equations (32) and (123) that the effective stiffness matrix $\bar{\mathbf{C}}_P^{(2)}$ for the pentamode metamaterial based on the representative cell in orientation # 2 shown in Figure 8b with the periodic boundary conditions listed in Equations (119)–(121) is given by

$$\begin{Bmatrix} \bar{\sigma}_{X_2 X_2} \\ \bar{\sigma}_{Y_2 Y_2} \\ \bar{\sigma}_{Z_2 Z_2} \\ \bar{\sigma}_{Y_2 Z_2} \\ \bar{\sigma}_{X_2 Z_2} \\ \bar{\sigma}_{X_2 Y_2} \end{Bmatrix} = \begin{bmatrix} \chi_{1P}^{(2)} & \chi_{2P}^{(2)} & \chi_{3P}^{(2)} & 0 & 0 & 0 \\ \chi_{2P}^{(2)} & \chi_{1P}^{(2)} & \chi_{3P}^{(2)} & 0 & 0 & 0 \\ \chi_{3P}^{(2)} & \chi_{3P}^{(2)} & \chi_{4P}^{(2)} & 0 & 0 & 0 \\ 0 & 0 & 0 & \chi_{6P}^{(2)} & 0 & 0 \\ 0 & 0 & 0 & 0 & \chi_{6P}^{(2)} & 0 \\ 0 & 0 & 0 & 0 & 0 & \chi_{5P}^{(2)} \end{bmatrix} \begin{Bmatrix} \bar{\epsilon}_{X_2 X_2} \\ \bar{\epsilon}_{Y_2 Y_2} \\ \bar{\epsilon}_{Z_2 Z_2} \\ \bar{\epsilon}_{Y_2 Z_2} \\ \bar{\epsilon}_{X_2 Z_2} \\ \bar{\epsilon}_{X_2 Y_2} \end{Bmatrix} = \bar{\mathbf{C}}_P^{(2)} \begin{Bmatrix} \bar{\epsilon}_{X_2 X_2} \\ \bar{\epsilon}_{Y_2 Y_2} \\ \bar{\epsilon}_{Z_2 Z_2} \\ \bar{\epsilon}_{Y_2 Z_2} \\ \bar{\epsilon}_{X_2 Z_2} \\ \bar{\epsilon}_{X_2 Y_2} \end{Bmatrix}, \tag{124}$$

where

$$\chi_{1P}^{(2)} = \frac{\sqrt{3}(k_a^2 + 7k_a k_s + k_s^2)}{12L(k_a + 2k_s)}, \quad \chi_{2P}^{(2)} = \frac{\sqrt{3}(k_a - k_s)^2}{12L(k_a + 2k_s)}, \quad \chi_{3P}^{(2)} = \frac{\sqrt{3}(k_a - k_s)}{12L}, \tag{125}$$

$$\chi_{4P}^{(2)} = \frac{\sqrt{3}(k_a + 2k_s)}{12L}, \quad \chi_{5P}^{(2)} = \frac{\sqrt{3}k_s}{2L}, \quad \chi_{6P}^{(2)} = \frac{3\sqrt{3}k_a k_s}{2L(k_a + 2k_s)}.$$

The compliance matrix $\bar{\mathbf{S}}_P^{(2)} = [\bar{\mathbf{C}}_P^{(2)}]^{-1}$ based on the representative cell in orientation # 2 with the periodicity constraints can then be readily obtained as

$$\bar{\mathbf{S}}_P^{(2)} = \begin{bmatrix} \zeta_{1P}^{(2)} & 0 & \zeta_{2P}^{(2)} & 0 & 0 & 0 \\ 0 & \zeta_{1P}^{(2)} & \zeta_{2P}^{(2)} & 0 & 0 & 0 \\ \zeta_{2P}^{(2)} & \zeta_{2P}^{(2)} & \zeta_{3P}^{(2)} & 0 & 0 & 0 \\ 0 & 0 & 0 & \zeta_{4P}^{(2)} & 0 & 0 \\ 0 & 0 & 0 & 0 & \zeta_{4P}^{(2)} & 0 \\ 0 & 0 & 0 & 0 & 0 & \zeta_{5P}^{(2)} \end{bmatrix}, \tag{126}$$

where

$$\zeta_{1P}^{(2)} = \frac{4\sqrt{3}L}{9} \left(\frac{2}{k_a} + \frac{1}{k_s} \right), \quad \zeta_{2P}^{(2)} = \frac{4\sqrt{3}L}{9} \left(\frac{1}{k_a} - \frac{1}{k_s} \right), \quad \zeta_{3P}^{(2)} = \frac{4\sqrt{3}L}{9} \left(\frac{1}{k_a} + \frac{2}{k_s} \right), \tag{127}$$

$$\zeta_{4P}^{(2)} = \frac{4\sqrt{3}L}{9} \left(\frac{1}{k_a} + \frac{1}{2k_s} \right), \quad \zeta_{5P}^{(2)} = \frac{2\sqrt{3}L}{3k_s}.$$

It can be readily shown that the effective stiffness and compliance matrices obtained in Equations (124) and (126) based on the representative cell in orientation # 2 can be

reproduced from those in Equations (115) and (117) based on the representative cell in orientation # 1 through a coordinate transformation given in Equations (106) and (107) with $\theta = -45^\circ$.

The engineering constants in this case with the periodicity constraints can be obtained from Equations (87)–(90), (115) and (116) as

$$\begin{aligned}\bar{E}_{per}(\theta) &= \frac{3\sqrt{3}k_a k_s}{2L[3(k_a+k_s)+(k_a-k_s)\cos(4\theta)]}, \\ \bar{G}_{per}(\theta) &= \frac{3\sqrt{3}k_a k_s}{8L[3k_a-2(k_a-k_s)\cos^2(2\theta)]}, \\ \bar{\nu}_{per}(\theta) &= \frac{(k_a-k_s)[1+\cos(4\theta)]}{3(k_a+k_s)+(k_a-k_s)\cos(4\theta)}.\end{aligned}\quad (128)$$

From Equation (128), it is seen that the effective engineering constants \bar{E}_{per} , \bar{G}_{per} and $\bar{\nu}_{per}$ do not show any dependency on the strut bending stiffness k_b , unlike the effective engineering constants \bar{E}_{hom} , \bar{G}_{hom} and $\bar{\nu}_{hom}$ given in Equation (91).

Note that Equations (91) and (128) can be further simplified to, with the help of Equations (4) and (5),

$$\begin{aligned}\bar{E}_{hom}(\theta) &= \frac{9\sqrt{3}\pi E d^4}{8L^2[3(16L^2+3d^2)+(16L^2-3d^2)\cos(4\theta)]}, \\ \bar{G}_{hom}(\theta) &= \frac{9\sqrt{3}\pi E d^4}{64L^2[24L^2-(16L^2-3d^2)\cos^2(2\theta)]}, \\ \bar{\nu}_{hom}(\theta) &= \frac{(16L^2-3d^2)[1+\cos(4\theta)]}{3(16L^2+3d^2)+(16L^2-3d^2)\cos(4\theta)}, \\ \bar{E}_{per}(\theta) &= \frac{9\sqrt{3}\pi E d^4}{8L^2[3(4L^2+3d^2)+(4L^2-3d^2)\cos(4\theta)]}, \\ \bar{G}_{per}(\theta) &= \frac{9\sqrt{3}\pi E d^4}{64L^2[6L^2-(4L^2-3d^2)\cos^2(2\theta)]}, \\ \bar{\nu}_{per}(\theta) &= \frac{(4L^2-3d^2)(\cos(4\theta)+1)}{3(4L^2+3d^2)+(4L^2-3d^2)\cos(4\theta)},\end{aligned}\quad (129)$$

$$\begin{aligned}\bar{E}_{per}(\theta) &= \frac{9\sqrt{3}\pi E d^4}{8L^2[3(4L^2+3d^2)+(4L^2-3d^2)\cos(4\theta)]}, \\ \bar{G}_{per}(\theta) &= \frac{9\sqrt{3}\pi E d^4}{64L^2[6L^2-(4L^2-3d^2)\cos^2(2\theta)]}, \\ \bar{\nu}_{per}(\theta) &= \frac{(4L^2-3d^2)(\cos(4\theta)+1)}{3(4L^2+3d^2)+(4L^2-3d^2)\cos(4\theta)},\end{aligned}\quad (130)$$

where d , L and E are the diameter, length and Young's modulus of the struts in the pentamode metamaterial.

By setting $r = d/L$, Equations (129) and (130) can be rewritten as

$$\begin{aligned}\frac{\bar{E}_{hom}(\theta)}{E} &= \frac{9\pi\sqrt{3}r^4}{8[3(16+3r^2)+(16-3r^2)\cos(4\theta)]}, & \frac{\bar{E}_{per}(\theta)}{E} &= \frac{9\pi\sqrt{3}r^4}{8[3(4+3r^2)+(4-3r^2)\cos(4\theta)]}, \\ \frac{\bar{G}_{hom}(\theta)}{E} &= \frac{9\pi\sqrt{3}r^4}{64[24+(3r^2-16)\cos^2(2\theta)]}, & \frac{\bar{G}_{per}(\theta)}{E} &= \frac{9\pi\sqrt{3}r^4}{64[6+(3r^2-4)\cos^2(2\theta)]}, \\ \bar{\nu}_{hom}(\theta) &= \frac{(16-3r^2)[1+\cos(4\theta)]}{3(16+3r^2)+(16-3r^2)\cos(4\theta)}, & \bar{\nu}_{per}(\theta) &= \frac{(4-3r^2)[1+\cos(4\theta)]}{3(4+3r^2)+(4-3r^2)\cos(4\theta)}.\end{aligned}\quad (131)$$

From Equation (131), it follows that

$$\begin{aligned}\frac{\bar{E}_{per}(\theta)}{\bar{E}_{hom}(\theta)} &= 1 + \frac{12[3+\cos(4\theta)]}{3(4+3r^2)+(4-3r^2)\cos(4\theta)}, & \frac{\bar{G}_{per}(\theta)}{\bar{G}_{hom}(\theta)} &= 1 + \frac{18-12\cos^2(2\theta)}{6-(4-3r^2)\cos^2(2\theta)}, \\ \frac{\bar{\nu}_{per}(\theta)}{\bar{\nu}_{hom}(\theta)} &= 1 + \frac{216r^2}{(-16+3r^2)[3(4+3r^2)+(4-3r^2)\cos(4\theta)]}.\end{aligned}\quad (132)$$

For $r < 1$, which is typical for most cellular structures, it can be readily verified that the first two ratios defined in Equation (132) are always greater than 1. This means that the homogenization with the periodicity constraints results in larger effective Young's and shear moduli than those without them. If $r \ll 1$, which is the case for Euler–Bernoulli beams, Equation (132) can be simplified to

$$\lim_{r \rightarrow 0} \frac{\bar{E}_{per}(\theta)}{\bar{E}_{hom}(\theta)} = \lim_{r \rightarrow 0} \frac{\bar{G}_{per}(\theta)}{\bar{G}_{hom}(\theta)} = 4, \quad \lim_{r \rightarrow 0} \frac{\bar{\nu}_{per}(\theta)}{\bar{\nu}_{hom}(\theta)} = 1. \quad (133)$$

Figure 11 shows the normalized effective engineering constants varying with $\theta \in [-90^\circ, 0]$. The numerical values are obtained from Equation (131) with $r = 1/(15\sqrt{3})$. It is seen that at $\theta = 0^\circ$ or -90° (i.e., the representative cell in orientation # 1 shown in Figure 8a), the effective Young's modulus is the smallest, the effective shear modulus is the largest, and the effective Poisson's ratio is nearly 0.5. However, at $\theta = -45^\circ$ (i.e., the representative cell in orientation # 2 shown in Figure 8b), the effective Young's modulus is the largest, the effective shear modulus is the smallest, and the effective Poisson's ratio reaches zero.

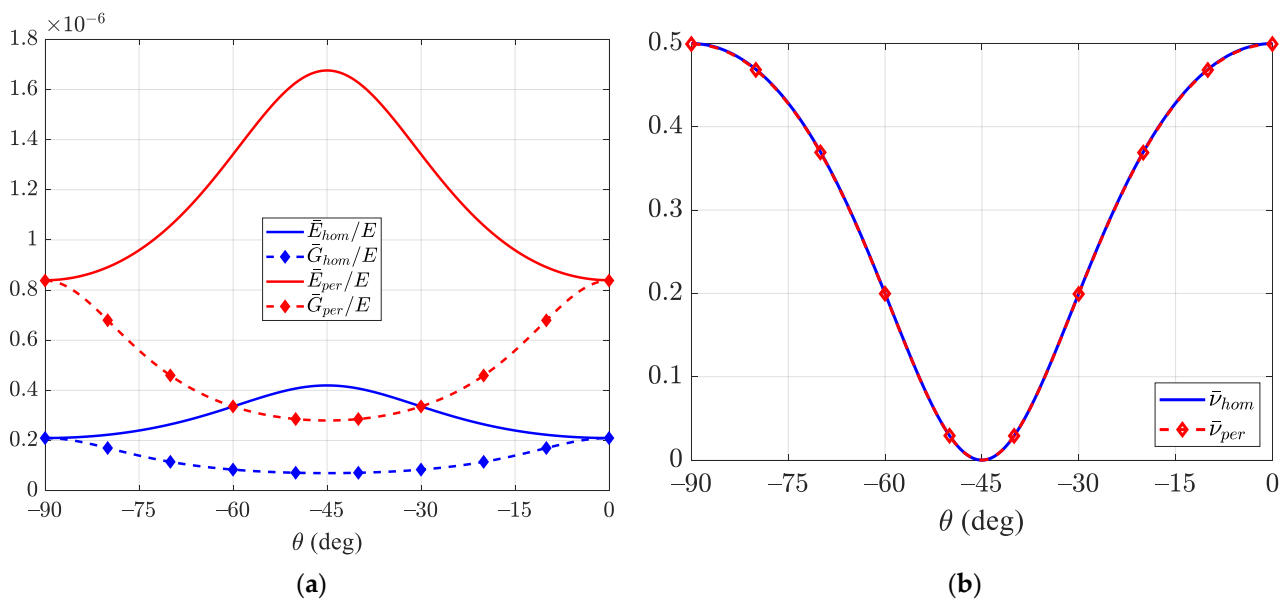


Figure 11. Variations of the effective engineering constants with θ : (a) Young's and shear moduli; (b) Poisson's ratio.

Figure 11 also reveals that both the effective Young's modulus and shear modulus of the pentamode metamaterial with the periodicity constraints are higher than those without the constraints for any orientation $\theta \in [-90^\circ, 0]$, while the effective Poisson's ratio is almost the same in the two cases for all orientations. The former reaffirms what has been qualitatively observed earlier from analyzing Equation (132).

In addition, the ratios given in Equation (132) are plotted in Figure 12. It is seen from Figure 12 that the smaller r ($= d/L$) is, the closer the results are to the limiting values listed in Equation (133), as expected. Moreover, it is observed from Figure 12 that the ratio of the effective shear moduli $\bar{G}_{per}/\bar{G}_{hom}$ does not depend on r at $\theta = -45^\circ$. This can also be directly seen from Equation (132), which analytically predicts $\bar{G}_{per}/\bar{G}_{hom} = 4$ at $\theta = -45^\circ$ for any value of r .

Furthermore, by setting $\theta = 0^\circ$ in Equation (128), the effective Poisson's ratio in the periodic case is obtained as

$$\bar{\nu}|_{\theta=0} = \frac{k_a - k_s}{2k_a + k_s}, \quad (134)$$

which clearly shows that the effective Poisson's ratio of the pentamode metamaterial based on the unit cell in orientation # 1 displayed in Figure 8a is controlled by the numerical values of the axial and shear stiffness constants of the strut. This indicates that auxetic pentamode metamaterials with $\bar{\nu} < 0$ can be obtained if struts with $k_s > k_a$ (i.e., the strut's shear stiffness being larger than its axial stiffness) are used. On the other hand, the same geometrical configuration of the struts can lead to a rubber-like material with $\bar{\nu} \cong 0.5$ if $k_a \gg k_s$ (i.e., the strut's axial stiffness being much larger than its shear stiffness—stretching dominated). These findings reveal that a full spectrum of Poisson's ratio can be attained by the pentamode metamaterial if struts are designed to have a tailorable ratio of k_a/k_s .

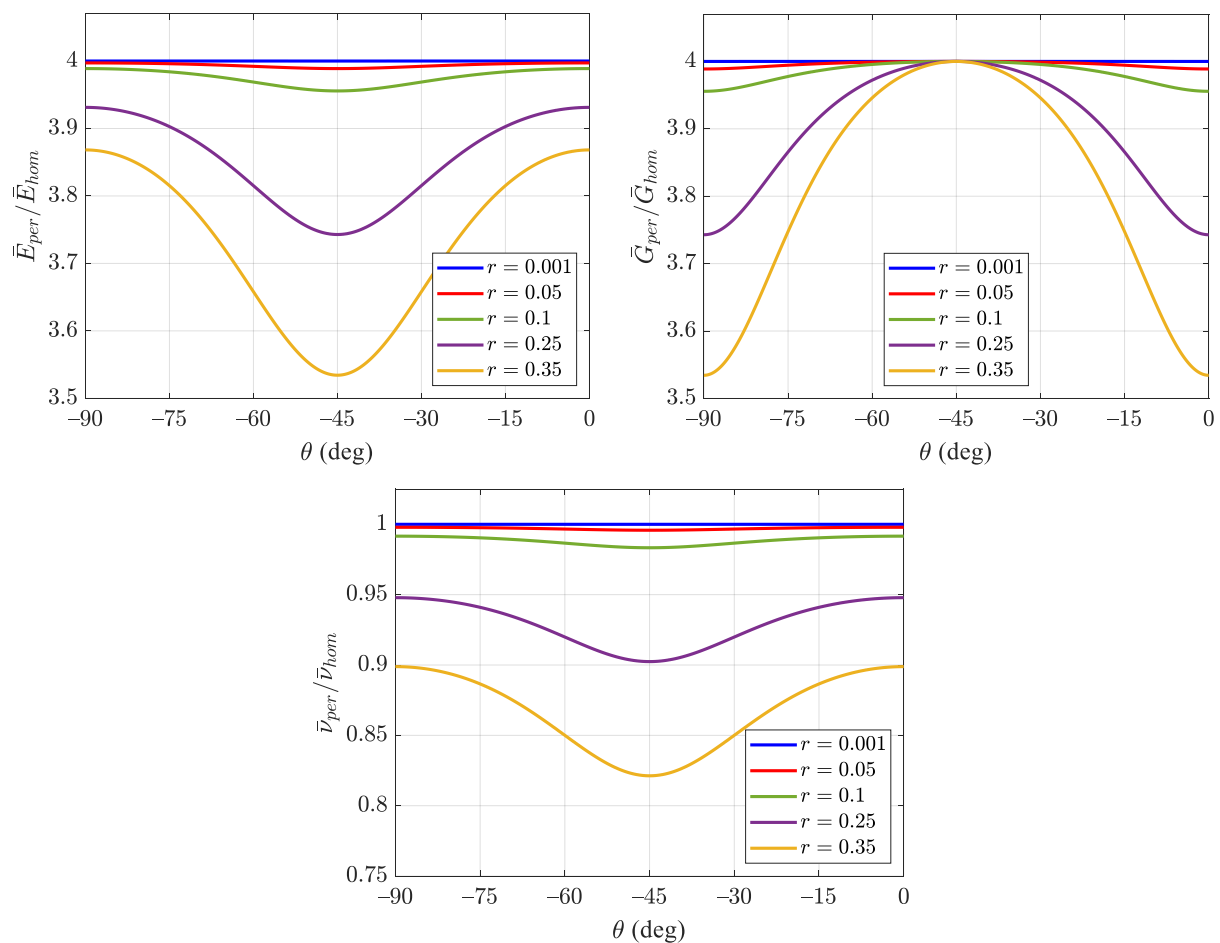


Figure 12. Variations of the engineering constant ratios with θ for various values of r .

4. Conclusions

A generalized strain energy-based homogenization method is provided for 2-D and 3-D cellular materials with and without periodicity constraints by using Hill's lemma and the matrix method for spatial frames. In the newly proposed homogenization method, the equilibrium equations are imposed at all boundary and interior nodes, and the interior nodes are allowed to translate and rotate without constraints, unlike in the existing strain energy-based methods that do not enforce the equilibrium conditions at the interior nodes. The new method can be applied to all types of 2-D and 3-D cellular structures with no geometrical constraints, which differs from the existing methods that can only be used to accurately predict effective elastic properties of cellular materials with symmetric or simple microstructures.

An asymmetric 2-D cellular material and a 3-D pentamode metamaterial, with and without periodicity constraints in each group, are homogenized by directly using the new method. In all four cases, closed-form expressions are obtained for the components of the effective stiffness matrix. For the 3-D pentamode metamaterial, the effective stiffness and compliance components are derived using two representative cells in two different orientations for both cases with and without periodicity constraints. The results based on the representative cell in one orientation show that the pentamode metamaterial displays the cubic symmetry and can be tailor-designed to be a rubber-like incompressible material or an auxetic material with a negative Poisson's ratio.

Finally, it should be mentioned that the effective stiffness matrix obtained without the periodic constraints has been found to be different from that acquired with the periodic constraints in each of the 2-D and 3-D homogenization examples considered. These analytical results attained using the newly proposed homogenization method need to

be compared with experimental data, when they become available, to further verify the new method and to determine which one, with or without the periodic constraints, is more accurate.

Author Contributions: Conceptualization, X.-L.G. and A.I.G.; Funding acquisition, X.-L.G.; Investigation, A.I.G. and X.-L.G.; Methodology, A.I.G. and X.-L.G.; Software, A.I.G.; Supervision, X.-L.G.; Validation, A.I.G. and X.-L.G.; Visualization, A.I.G.; Writing—original draft, A.I.G.; Writing—review & editing, X.-L.G. All authors have read and agreed to the published version of the manuscript.

Funding: X.-L.G. gratefully acknowledges the support by SMU through the Gerald J. Ford Research Fellowship.

Institutional Review Board Statement: Not applicable.

Informed Consent Statement: Not applicable.

Acknowledgments: The authors would like to thank Teik-Cheng Lim and two anonymous reviewers for their encouragement and helpful comments on an earlier version of the paper.

Conflicts of Interest: The authors declare no conflict of interest.

References

- Hassani, B.; Hinton, E. A review of homogenization and topology optimization I—homogenization theory for media with periodic structure. *Comput. Struct.* **1998**, *69*, 707–717. [[CrossRef](#)]
- Arabnejad, S.; Pasini, D. Mechanical properties of lattice materials via asymptotic homogenization and comparison with alternative homogenization methods. *Int. J. Mech. Sci.* **2013**, *77*, 249–262. [[CrossRef](#)]
- Bacigalupo, A.; Gambarotta, L. Homogenization of periodic hexa- and tetrachiral cellular solids. *Compos. Struct.* **2014**, *116*, 461–476. [[CrossRef](#)]
- Iltchev, A.; Marcadon, V.; Kruch, S.; Forest, S. Computational homogenisation of periodic cellular materials: Application to structural modelling. *Int. J. Mech. Sci.* **2015**, *93*, 240–255. [[CrossRef](#)]
- Lim, T.C. *Auxetic Materials and Structures*; Springer: Singapore, 2015.
- Ai, L.; Gao, X.-L. Three-dimensional metamaterials with a negative Poisson's ratio and a non-positive coefficient of thermal expansion. *Int. J. Mech. Sci.* **2018**, *135*, 101–113. [[CrossRef](#)]
- Ongaro, F. Estimation of the effective properties of two-dimensional cellular materials: A review. *Theor. Appl. Mech. Lett.* **2018**, *8*, 209–230. [[CrossRef](#)]
- Xu, H.; Farag, A.; Pasini, D. Routes to program thermal expansion in three-dimensional lattice metamaterials built from tetrahedral building blocks. *J. Mech. Phys. Solids* **2018**, *117*, 54–87. [[CrossRef](#)]
- Lim, T.-C. *Mechanics of Metamaterials with Negative Parameters*; Springer Nature: Singapore, 2020.
- Lim, T.-C. An Auxetic system based on interconnected Y-elements inspired by Islamic geometric patterns. *Symmetry* **2021**, *13*, 865. [[CrossRef](#)]
- Gad, A.; Gao, X.-L.; Li, K. A strain energy-based homogenization method for 2-D and 3-D cellular materials using the micropolar elasticity theory. *Compos. Struct.* **2021**, *265*, 113594. [[CrossRef](#)]
- Warren, W.E.; Kraynik, A.M. Linear elastic behavior of a low-density Kelvin foam with open cells. *J. Appl. Mech.* **1997**, *64*, 787–794. [[CrossRef](#)]
- Tollenaere, H.; Caillerie, D. Continuous modeling of lattice structures by homogenization. *Adv. Eng. Softw.* **1998**, *29*, 699–705. [[CrossRef](#)]
- Li, K.; Gao, X.-L.; Roy, A.K. Micromechanics model for three-dimensional open-cell foams using a tetrakaidecahedral unit cell and Castigliano's second theorem. *Compos. Sci. Technol.* **2003**, *63*, 1769–1781. [[CrossRef](#)]
- Demiray, S.; Becker, W.; Hohe, J. Strain-energy based homogenisation of two- and three-dimensional hyperelastic solid foams. *J. Mater. Sci.* **2005**, *40*, 5839–5844. [[CrossRef](#)]
- Martinsson, P.G.; Babuška, I. Homogenization of materials with periodic truss or frame micro-structures. *Math. Model. Methods Appl. Sci.* **2007**, *17*, 805–832. [[CrossRef](#)]
- Freund, J.; Karakoc, A.; Sjolund, J. Computational homogenization of regular cellular material according to classical elasticity. *Mech. Mater.* **2014**, *78*, 56–65. [[CrossRef](#)]
- Norris, A.N. Mechanics of elastic networks. *Proc. R. Soc. A* **2014**, *470*, 20140522. [[CrossRef](#)]
- Ongaro, F.; Barbieri, E.; Pugno, N. Mechanics of mutable hierarchical composite cellular materials. *Mech. Mater.* **2018**, *124*, 80–99. [[CrossRef](#)]
- Ai, L.; Gao, X.-L. An analytical model for star-shaped re-entrant lattice structures with the orthotropic symmetry and negative Poisson's ratios. *Int. J. Mech. Sci.* **2018**, *145*, 158–170. [[CrossRef](#)]
- Evans, K.E.; Alderson, A. Auxetic materials: Functional materials and structures from lateral thinking. *Adv. Mater.* **2000**, *12*, 617–628. [[CrossRef](#)]

22. Lakes, R.; Wojciechowski, K.W. Negative compressibility, negative Poisson's ratio, and stability. *Phys. Status Solidi (b)* **2008**, *245*, 545–551. [[CrossRef](#)]
23. Greaves, G.N.; Greer, A.L.; Lakes, R.S.; Rouxel, T. Poisson's ratio and modern materials. *Nat. Mater.* **2011**, *10*, 823–837. [[CrossRef](#)] [[PubMed](#)]
24. Lakes, R.S. Negative-Poisson's-ratio materials: Auxetic solids. *Annu. Rev. Mater. Res.* **2017**, *47*, 63–81. [[CrossRef](#)]
25. Ai, L.; Gao, X.-L. Metamaterials with negative Poisson's ratio and non-positive thermal expansion. *Compos. Struct.* **2017**, *162*, 70–84. [[CrossRef](#)]
26. Ai, L.; Gao, X.-L. Micromechanical modeling of 3D printable interpenetrating phase composites with tailorable effective elastic properties including negative Poisson's ratio. *J. Micromech. Mol. Phys.* **2017**, *2*, 1750015. [[CrossRef](#)]
27. Czarnecki, S.; Łukasiak, T. Recovery of the auxetic microstructures appearing in the least compliant continuum two-dimensional bodies. *Phys. Status Solidi (B)* **2020**, *257*, 1900676. [[CrossRef](#)]
28. Askar, A.; Cakmak, A. A structural model of a micropolar continuum. *Int. J. Eng. Sci.* **1968**, *6*, 583–589. [[CrossRef](#)]
29. Bažant, Z.; Christensen, M. Analogy between micropolar continuum and grid frameworks under initial stress. *Int. J. Solids Struct.* **1972**, *8*, 327–346. [[CrossRef](#)]
30. Chen, J.; Huang, Y.; Ortiz, M. Fracture analysis of cellular materials: A strain gradient model. *J. Mech. Phys. Solids* **1998**, *46*, 789–828. [[CrossRef](#)]
31. Wang, X.L.; Stronge, W.J. Micropolar theory for two—Dimensional stresses in elastic honeycomb. *Proc. R. Soc. A Math. Phys. Eng. Sci.* **1999**, *455*, 2091–2116. [[CrossRef](#)]
32. Kumar, R.S.; McDowell, D.L. Generalized continuum modeling of 2-D periodic cellular solids. *Int. J. Solids Struct.* **2004**, *41*, 7399–7422. [[CrossRef](#)]
33. Park, S.K.; Gao, X.-L. Micromechanical modeling of honeycomb structures based on a modified couple stress theory. *Mech. Adv. Mater. Struct.* **2008**, *15*, 574–593. [[CrossRef](#)]
34. Bacigalupo, A.; Gambarotta, L. Generalized micropolar continualization of 1D beam lattices. *Int. J. Mech. Sci.* **2019**, *155*, 554–570. [[CrossRef](#)]
35. Niu, B.; Yan, J. A new micromechanical approach of micropolar continuum modeling for 2-D periodic cellular material. *Acta Mech. Sin.* **2016**, *32*, 456–468. [[CrossRef](#)]
36. Weaver, W.; Gere, J.M. *Matrix Analysis of Framed Structures*, 3rd ed.; Springer: New York, NY, USA, 1990.
37. Li, K.; Gao, X.-L.; Roy, A. Micromechanical modeling of three-dimensional open-cell foams using the matrix method for spatial frames. *Compos. Part B Eng.* **2005**, *36*, 249–262. [[CrossRef](#)]
38. Hill, R. Elastic properties of reinforced solids: Some theoretical principles. *J. Mech. Phys. Solids* **1963**, *11*, 357–372. [[CrossRef](#)]
39. Gao, X.-L. Extended Hill's lemma for non-Cauchy continua based on the simplified strain gradient elasticity theory. *J. Micromech. Mol. Phys.* **2016**, *3*, 1640004. [[CrossRef](#)]
40. Gad, A.I.; Gao, X.-L. Extended Hill's lemma for non-Cauchy continua based on a modified couple stress theory. *Acta Mech.* **2020**, *231*, 977–997. [[CrossRef](#)]
41. Gad, A.I.; Gao, X.-L. Two versions of the extended Hill's lemma for non-Cauchy continua based on the couple stress theory. *Math. Mech. Solids* **2021**, *26*, 244–262. [[CrossRef](#)]
42. Li, S.; Wang, G. *Introduction to Micromechanics and Nanomechanics*; World Scientific: Singapore, 2008.
43. Liu, Q. Hill's lemma for the average-field theory of Cosserat continuum. *Acta Mech.* **2013**, *224*, 851–866. [[CrossRef](#)]
44. Warren, W.E.; Kraynik, A.M. The linear elastic properties of open-cell foams. *J. Appl. Mech.* **1988**, *55*, 341–346. [[CrossRef](#)]
45. Drago, A.; Pindera, M.J. Micro-macromechanical analysis of heterogeneous materials: Macroscopically homogeneous vs periodic microstructures. *Compos. Sci. Technol.* **2007**, *67*, 1243–1263. [[CrossRef](#)]
46. Liu, Q. A new version of Hill's lemma for Cosserat continuum. *Arch. Appl. Mech.* **2015**, *85*, 761–773. [[CrossRef](#)]
47. Bilski, M.; Piękowski, P.; Wojciechowski, K. Extreme Poisson's ratios of honeycomb, re-entrant, and zig-zag crystals of binary hard discs. *Symmetry* **2021**, *13*, 1127. [[CrossRef](#)]
48. Milton, G.W.; Cherkaev, A.V. Which elasticity tensors are realizable? *J. Eng. Mater. Technol.* **1995**, *117*, 483–493. [[CrossRef](#)]
49. Hayes, M. Connexions between the moduli for anisotropic elastic materials. *J. Elast.* **1972**, *2*, 135–141. [[CrossRef](#)]
50. Norris, A.N. Poisson's ratio in cubic materials. *Proc. R. Soc. A* **2006**, *462*, 3385–3405. [[CrossRef](#)]
51. Ting, T.C.T. *Anisotropic Elasticity—Theory and Applications*; Oxford University Press: New York, NY, USA, 1996.